Weathering fluxes and sediment provenance on the SW Scottish shelf during the last deglaciation

Riccardo Arosio[a,*], Kirsty C. Crocket[a], Geoffrey M. Nowell[b], S. Louise Callard[c], John A. Howe[a], Sara Benetti[d], Derek Fabel[e], Steve Moreton[f], Chris D. Clark[g]

[a] Scottish Association for Marine Science, Oban PA37 1QA, UK
[b] NCIET, University of Durham, South Road, Durham DH1 3LE, UK
[c] Department of Geography, University of Durham, Durham DH1 3LE, UK
[d] School of Environmental Sciences, University of Ulster, Coleraine BT52 1SA, UK
[e] Scottish Universities Environmental Research Centre, East Kilbride G75 0QF, UK
[f] NERC Radiocarbon Facility, East Kilbride G75 0QF, UK
[g] Department of Geography, University of Sheffield, Sheffield S10 2TN, UK

ABSTRACT

The reconstruction of past ice sheet dynamics can inform on long-term ice stream activity, and in turn provide constraints on the response of modern ice sheets to climate change. The Hebrides Ice Stream (HIS) flowed across part of the western Scottish shelf to the shelf-break during the last glacial cycle. To investigate the deglacial dynamics of the HIS following the Last Glacial Maximum (LGM), lead (Pb) isotope records were extracted from the FeMn oxyhydroxide and detrital fractions of recovered laminated glacimarine mud sequences to monitor the changing activity of HIS during its retreat. These provide, respectively, relative timing of glacially weathered inputs to the marine environment and some source information on the eroded sediments. The FeMn oxyhydroxide fraction is dominated by pre-formed particles and shows a marked decrease from radiogenic at ~ 21 cal ka to less radiogenic Pb isotope compositions towards 15.4–13 ka. This decrease represents a reduction in the flux of subglacially-derived radiogenic Pb to the continental shelf, and it is interpreted as the result of the break-up of the ice-stream in western Scotland around that time. The Pb, Sr and Nd isotopic signatures of the detrital fraction indicate a preponderance of fine sediments originated from the NW Highlands throughout the period studied (~ 21 to 15 cal ka BP), most likely dictated by the orientation of tidal and oceanic current directions and sediment delivery. Both fractions show inversion of the $^{208}Pb/^{204}Pb$ ratio relative to the other Pb isotope ratios. This is observed only in one core site in the detrital fraction, and extended to all cores in the FeMn oxyhydroxide fraction. This behaviour highlights the influence of ocean currents in restricting the detrital but encouraging dispersal of the FeMn oxyhydroxide signal. Periodic increased contributions from a high Th/U source, potentially the neighbouring Archaean amphibolitic Lewisian basement in the Outer Hebrides, are proposed as the source of these $^{208}Pb/^{204}Pb$ inversions. This study demonstrates how geochemical investigation on continental shelves can be used to constrain the activity and flow sources of palaeo-ice streams, and the utility of combining detrital and FeMn oxyhydroxides to determine the combined influence of the continental sources of material and their dispersal in the marine environment.

1. Introduction

Current global climate change is disrupting the stability of large, polar ice sheets, which in turn affect global sea level and ocean circulation. Already Joughin et al. (2002), Cook (2005), Pritchard et al. (2009), Joughin et al. (2014) and other studies have shown recent and ongoing alterations in polar ice masses, including variations in ice stream flow, rapid ice mass thinning, ice stream frontal retreat, and changes in subglacial regimes. Understanding these dynamics is of great importance to predict future global changes, and increasing emphasis

has been placed on studying physical processes at the ice–ocean interface, both in modern and palaeo-ice sheet settings, to determine how these processes affect ice-sheet stability (Carr et al., 2015; Jamieson et al., 2014; Patton et al., 2016).

In order to improve the accuracy of ice-sheet model projections, a better understanding of the relationship between palaeoclimate and long timescale dynamics of palaeo-ice sheets and ice streams is indispensable. In this context, the mid-latitude and mostly marine-terminating British-Irish Ice Sheet (BIIS) is a good case study, due to its sensitivity to oceanic and climatic variations. At the Last Glacial
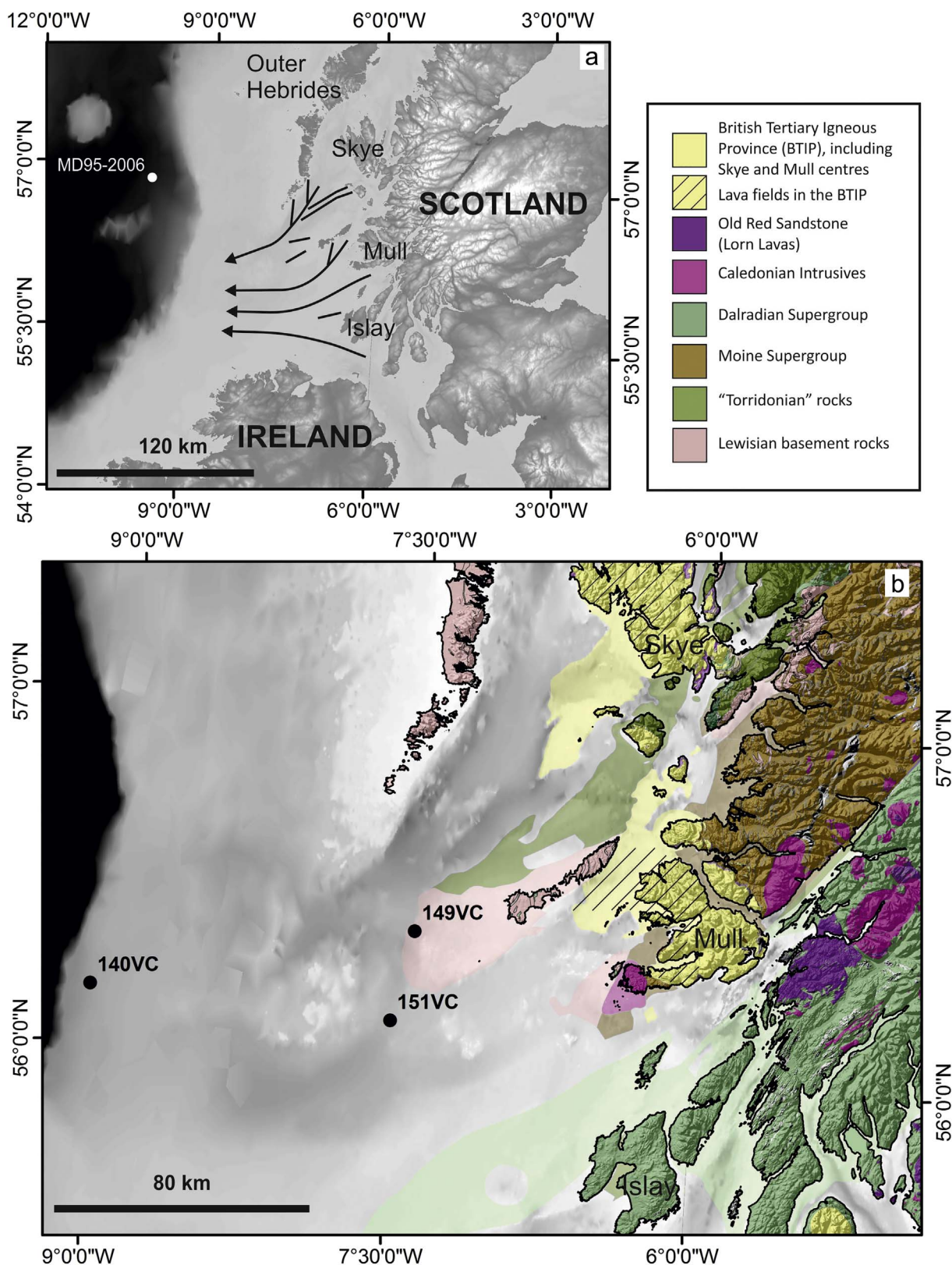
Fig. 1. a) Regional overview of the study area. The map shows the flow model of the Hebrides Ice Stream during its main stage (~27–24 ka, modified after Dove et al., 2015). b) Geological map of Western Scotland and location of the three cores sampled. Main geological groups are shown with different colours and average Pb isotope ratios are provided (modified after Emeleus and Bell (2005)). (For interpretation of the references to colour in this figure legend, the reader is referred to the web version of this article.)

Maximum (LGM) the BIIS advanced onto the continental shelf and ice-streams developed in different locations along its margin, causing an increased discharge of terrigenous ice-rafted debris (IRD), meltwater and suspended sediment into the open ocean (Broecker et al., 1992;

Hemming, 2004; Scourse et al., 2009). One example is the Hebrides Ice Stream (HIS) (also known as Barra or Barra-Donegal Ice Stream), which occupied the western Scottish and north Irish portion of BIIS and was characterised by purge events at different times during deglaciation
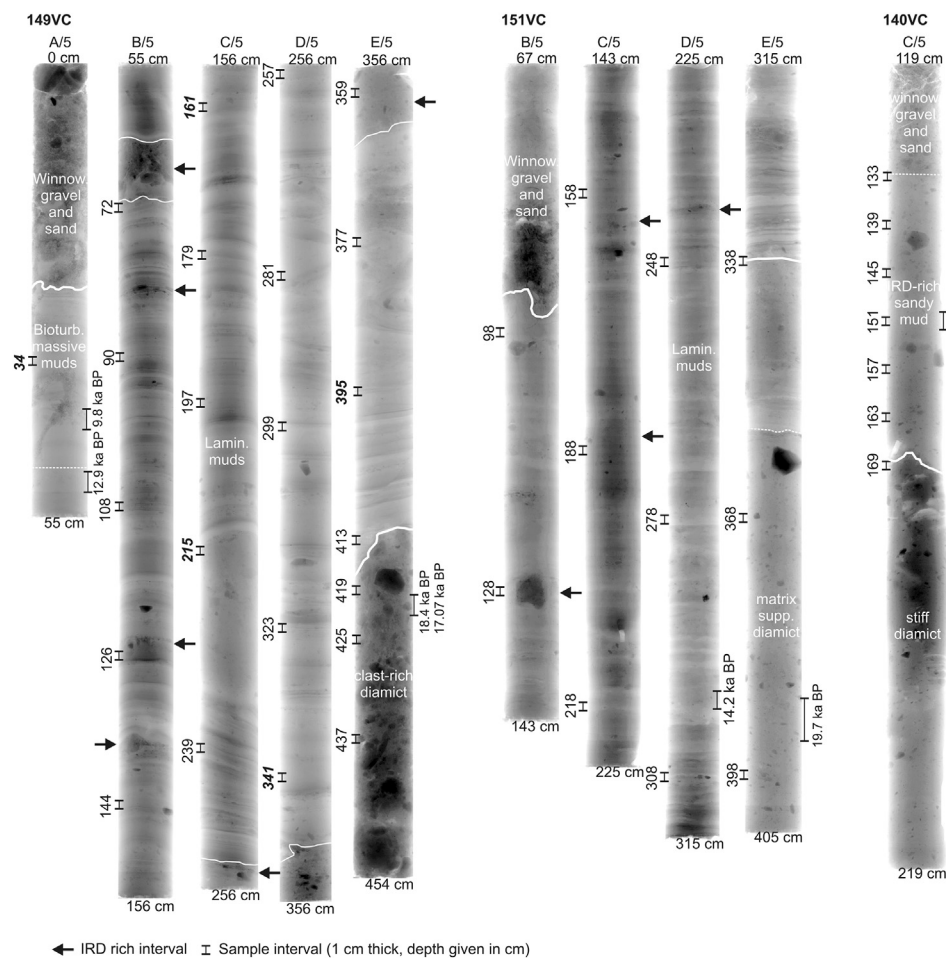
Fig. 2. X-ray photographs of the core sections analysed. A summarised stratigraphy and the sampled intervals are provided. In core 149, sample intervals in ***bold + italics*** belong to group G3; sample intervals from 419 downwards belong to group G1, and all the others belong to group G2. In core 151 sample intervals from 308 downwards belong to G1, the rest belong to G2 (see Discussion).

(Knutz et al., 2001; Scourse et al., 2009; Wilson et al., 2002).

The sources of glacially eroded sediment at different times can be used to reconstruct and to better constrain the activity and demise of ice sheets. Lead isotope ratios as a tracer of detrital catchments in the North Atlantic are well established. For example, the nature and provenance of Heinrich layers have been investigated by measuring Pb isotopes ratios on feldspar grains (Farmer et al., 2003; Gwiazda et al., 1996a, 1996b; Hemming, 2004). Extensive studies on bulk < 63 μm sediments from deep-sea cores have also proved very useful in discriminating source areas for detrital supplies (Bailey et al., 2013; Fagel et al., 2002; Farmer et al., 2003; Maccali et al., 2012; von Blanckenburg and Nägler, 2001). Complementary to the detrital investigations, the Pb isotopic composition in marine authigenic precipitates are employed to re-construct water mass circulation and continental weathering fluxes (Crocket et al., 2012; Foster and Vance, 2006; Gutjahr et al., 2009; Kurzweil et al., 2010; von Blanckenburg and Nägler, 2001). The dissolved Pb isotope composition in the water column is determined by the style of continental physical erosion and chemical weathering (Christensen et al., 1997; von Blanckenburg and Nägler, 2001) as a result of the preferential release of radiogenic Pb, relative to common Pb, during the incipient stages of continental chemical weathering (Erel and Morgan, 1992; Harlavan and Erel, 2002). The lead isotope composition of seawater is preserved in authigenic deposits, for example authigenic FeMn oxyhydroxides, that can be separated and studied using a selective leaching technique (Gutjahr et al., 2007, 2009). The variation in Pb isotope composition of these Fe-Mn rich marine deposits can in turn be associated with increased continental export fluxes through iceberg calving at ice sheet margins. As the FeMn oxyhydroxides are carried in the dissolved and suspended phases, they can potentially have a different spatial impact than IRD.

Little work has been done on applying Pb radiogenic isotopes to reconstruct ice stream activity within individual sections of ice sheets. In the context of the BIIS, Crocket et al. (2013) showed a high resolution authigenic Fe-Mn Pb signature from ODP Site 980 (Feni Drift, NE Atlantic) that records the activity of the western sector of the BIIS, and in particular the HIS during the last 43 ka. However the local variations in the HIS cannot be resolved due to the regionally integrated Pb isotope signal in the Site 980 record. Single ice-sheet studies can be useful to reconstruct local ice sheet decay, link the decay to changes in climate and oceanographic conditions, and predict how future climate and oceanographic boundary conditions will affect existing ice sheets. This study is the first application of Pb isotope compositions, complemented by Sr and Nd isotope ratios and major/trace element analyses, to three sediment cores from the continental shelf offshore western Scotland to identify changes both in detrital supplies to shelf sediments and variations in glacial weathering fluxes that occurred since ~21 ka. We combine analysis of both the FeMn oxyhydroxide and detrital fractions to reveal the regional influences of continental source inputs of IRD and the weathered inputs in the suspended and dissolved phases. These results contribute to the understanding of the timing of HIS activity, especially in terms of ice sheet dynamics and increased meltwater fluxes. The results are complemented by geomorphological and stratigraphical evidence on the shelf (Dove et al., 2015; Dunlop et al., 2010; Howe et al., 2012).

Table 1
BRITICE-CHRONO key core location data.

Core ID	Type	Latitude (N)	Longitude (W)	Water depth (m)	Core length (m)
JC106_140VC	Vibrocore	56° 10.164′	9° 04.010′	167	4.18
JC106_149VC	Vibrocore	56° 23.83′	7° 26.928′	136	4.5
JC106_151VC	Vibrocore	56° 8.427′	7° 32.263′	112	4.1

2. Sampling sites and sedimentology

Three vibrocores (JC106_140VC, JC106_149VC and JC106_151VC, hereafter referred to as 140, 149 and 151 respectively) collected during the 2014 BRITICE-CHRONO cruise on board of the RRS James Cook in the Malin Sea were chosen amongst 40 others on the basis of their geographical position, sedimentology and length (Figs. 1, 2 and Table 1). Core 140 was collected close to the shelf edge and the Barra-Donegal Fan. The upper units consist of layers of winnowed sand and shelly gravel (0–0.74 m in the core) underlain by soft and massive pebbly sandy mud (0.74–1.27). The basal 3 m (1.27–4.18 m) consist of matrix-supported diamicton in a clay matrix, with stiffness increasing downcore (shear strength from 47.5 kPa at 1.3 m to a maximum of 167.5 kPa towards the base). The interval between 1.27 and 1.7 m of this firm diamicton records iceberg-turbated distal glacimarine deposition after the LGM (based on the shear strength values and post-LGM date, see Section 4.2; Shipp et al., 2002), while the stiffer and darker diamicton between 1.7 and 4.18 m is interpreted as subglacial till (Evans et al., 2006; see also Chronostratigraphy). Cores 149 and 151 were collected on the mid-shelf W and SSW respectively of the Isle of Tiree (Fig. 1). These cores are located at approximately the same longitude but different latitude in order to monitor the competing influence of the two branches of the HIS after the LGM. Core 151 consists of approximately ~4 m of laminated glacimarine mud with a basal IRD-rich massive mud unit between ~3.4 and 4 m. Isolated cm-mm (Fig. 2) thick IRD rich layers occur periodically within the laminated glacimarine muds. Core 149 has instead a ~4 m succession of finely laminated glacimarine muds, with IRD-rich intervals overlaying a firm diamicton with a sandy mud matrix unit. The diamicton might represent either an ice-contact or a thick ice-rafted deposit (Evans et al., 2006).

3. Source catchment geochemistry

Scotland is characterised by a complex and varied geology, with progressively more ancient (from South to North) metamorphic Dalradian (~0.7 Ga), Moine (~1.1 Ga) and Lewisian (~2.9 Ga) terranes, bound by major fault systems (Trewin, 2002). Prominent igneous centres of Palaeogene age (~55 Ma, the British Tertiary Igneous

Provinces) occupy large portions of Skye, Rum, Eigg, Mull and the Ardnamurchan peninsula. A survey of the published material on Pb isotope ratios from bulk rock samples in western Scotland was carried out for this study. The dataset is summarised in a schematic representation of the main source catchments, geology and average isotope ratios (Figs. 1, 9 and Table A2.9, Supplementary material).

Unfortunately, the existing Pb isotope determinations are geographically uneven. The Pb isotope ratios of Palaeogene and Caledonian Igneous intrusions and extrusions are the best established. Less extensive are the studies on the Pb compositions of bulk Lewisian crust. On the other hand, there are relatively few analyses of the isotopic composition of the great metasedimentary terranes of the Proterozoic-Cambrian, i.e. the Moine and Dalradian Supergroups. A second issue arises when considering the geographical position of Palaeogene centres. As coeval sources, and in this case probably derived from the same mantle-derived reservoirs, they are likely to have very similar isotope ratios. While there is indeed juxtaposition between the igneous rocks of Skye and Mull, differences caused by contamination by crustal-derived elements during magma emplacement (Dickin, 1981; Kerr et al., 1995) might be helpful in discriminating between the two sources.

Several studies (e.g. Clark, 1987; Farmer et al., 2003) have shown how fine-grained material in glacimarine cores derives from glacial abrasion, associated with melting and refreezing (Benn and Evans, 2010), of local crustal rocks (up to 100 km distance), rather than sediment from the interiors of the ice-sheets. However, good mixing of meltwater plumes and the water column could transport material further (Andrews and Syvitski, 1994), especially with a tidal regime that was thought to be stronger along western Scotland's marine margin during deglaciation (Ward et al., 2016). Taking into account the position of the ice divides after the LGM and the reconstructed activity of the ice streams acting after ~20 ka (C.D. Clark et al., 2012; J. Clark et al., 2012; Dove et al., 2015; Finlayson et al., 2014; McCabe and Williams, 2012), only sources from western Scotland are therefore considered in this study. Sources external to Britain and Ireland are assumed to have an insignificant influence on the geochemical composition of the detrital material on the mid-interior UK shelf.

4. Materials and methods

The Pb isotope composition was measured in the authigenic FeMn oxyhydroxide (n = 37) and detrital (n = 40) fractions (Table 3a). The Sr and Nd isotope compositions for selected samples of the detrital fraction of core 149 were also analysed (12 in total). Major and trace elements were measured for all the samples in cores 149 and 140. Samples were collected from at least 30 cm below the seafloor, minimising anthropogenic Pb contamination and avoiding superficial units of sediment not belonging to the Late-Devensian period. The Pb analytical procedures followed the technique applied in Crocket et al. (2012) and adapted from Gutjahr et al. (2007).

Table 2
AMS ^{14}C dates. Calib 7.1 uses an assumed ~400 year global surface water average marine reservoir effect (MRE) offset for radiocarbon ages calibrated using the Marine13 calibration curves. In this instance the marine reservoir offset was not modified with a local-temporal offset (ΔR) as our knowledge of the residence time of ^{14}C in the ocean during the LGM to Holocene is poorly constrained. Evidence from the North Atlantic (e.g. Austin et al., 1995; Thornalley et al., 2011), indicates that the marine reservoir effect would have been considerably higher during the last termination to Holocene. A consequence of applying a larger MRE correction would be younger calibrated ages. Errors are given at 2σ.

Lab. code	Core ID	Metres (bsf)	Material	^{14}C age (year BP)	Corr. age (cal year BP)
UBA-29958	149VC	0.4	*Nucula sulcata*	9873 ± 40	10,835 ± 160
UBA-29138	149VC	0.51	Bivalve fragment	12,951 ± 48	14,807 ± 320
UBA-29959	149VC	2.2	Bivalve fragment	9501 ± 46	10,356 ± 130
UBA-29960	149VC	4.2	Bivalve fragment	18,441 ± 94	21,864 ± 300
SUERC-59509	149VC	4.21	Bivalve fragment	17,077 ± 56	20,119 ± 202
UBA-29135	140VC	0.96	*Hiatella arctica*	10,707 ± 56	12,145 ± 268
UBA-29136	140VC	1.51	*Yoldiella* sp.	18,236 ± 102	21,583 ± 308
UBA-29137	140VC	2.99	Bivalve fragment	50,780 ± 2520	No calib.
SUERC-67939	151VC	3.00–3.02	*Yoldiella* sp.	14,269 ± 46	16,782 ± 228
UCIAMS-179841	151VC	3.89–3.94	Foramin. (mixed)	19,690 ± 90	23,233 ± 283

Table 3a

Pb concentration and isotope ratios from both detrital and leachate fractions in the three sediment cores. Each sample corresponds to an analytical session (Session No) presented in Table 3b.

ID	Session No	[Pb] µg/g	206Pb/204Pb	2SE	207Pb/204Pb	2SE	208Pb/204Pb	2SE	207Pb/206Pb	2SE	208Pb/206Pb	2SE
JC106_140VC												
Leachate												
αC1r	5	6.422	19.70540	0.00057	15.74429	0.00054	38.52297	0.00162	0.79899	0.00001	1.95497	0.00003
αC2	4	6.993	19.72486	0.00074	15.74438	0.00074	38.50547	0.00221	0.79820	0.00001	1.95213	0.00005
αC4	4	6.070	19.68570	0.00069	15.73944	0.00072	38.52269	0.00226	0.79955	0.00001	1.95692	0.00006
αC6	4	5.978	19.72553	0.00082	15.74508	0.00080	38.48789	0.00242	0.79820	0.00001	1.95116	0.00005
αC7r	5	6.165	19.58900	0.00048	15.73011	0.00049	38.54557	0.00132	0.80301	0.00001	1.96772	0.00003
Replicates (re-sampled)												
αC4r	5	6.676	19.77622	0.00062	15.75308	0.00056	38.49733	0.00162	0.79657	0.00001	1.94666	0.00004
Detrital												
αC1	4	2.411	18.97783	0.00067	15.62351	0.00067	38.62366	0.00211	0.82326	0.00001	2.03518	0.00006
αC2	4	3.014	19.06874	0.00059	15.64550	0.00066	38.68113	0.00217	0.82049	0.00001	2.02853	0.00006
αC3	4	3.171	19.03791	0.00068	15.63914	0.00071	38.69103	0.00232	0.82148	0.00001	2.03230	0.00006
αC4	4	3.060	19.07305	0.00068	15.64360	0.00076	38.82433	0.00224	0.82019	0.00002	2.03557	0.00006
αC5	4	2.963	19.02746	0.00073	15.63271	0.00077	38.67805	0.00252	0.82158	0.00001	2.03275	0.00006
αC6	4	2.818	19.06138	0.00069	15.63630	0.00076	38.65936	0.00212	0.82030	0.00001	2.02814	0.00005
αC7	4	2.717	18.93889	0.00081	15.62445	0.00068	38.68124	0.00248	0.82500	0.00001	2.04250	0.00007
JC106_149VC												
Leachate												
βA5r	5	13.034	19.56935	0.00058	15.72516	0.00055	38.55684	0.00159	0.80357	0.00001	1.97027	0.00003
βB3	2	9.218	19.49597	0.00072	15.71689	0.00074	38.56615	0.00229	0.80617	0.00002	1.97816	0.00006
βB6	2	7.086	19.51211	0.00076	15.71997	0.00083	38.55410	0.00266	0.80565	0.00002	1.97589	0.00007
βB9r	5	10.571	19.57094	0.00054	15.72552	0.00055	38.54878	0.00157	0.80350	0.00001	1.96968	0.00003
βB12	2	8.255	19.62230	0.00095	15.73332	0.00101	38.52632	0.00308	0.80181	0.00001	1.96341	0.00007
βB15	5	6.156	19.49647	0.00112	15.71867	0.00101	38.57521	0.00302	0.80621	0.00002	1.97854	0.00006
βC1r	2	15.182	19.48130	0.00057	15.71501	0.00057	38.60711	0.00169	0.80666	0.00001	1.98173	0.00004
βC4	2	5.537	19.57919	0.00084	15.72919	0.00096	38.57055	0.00300	0.80333	0.00002	1.96998	0.00008
βC7	3	6.877	19.59649	0.00091	15.72736	0.00095	38.57686	0.00302	0.80255	0.00001	1.96854	0.00007
βC14	3	8.848	19.61334	0.00088	15.73111	0.00091	38.56370	0.00280	0.80206	0.00001	1.96617	0.00006
βD1	3	6.687	19.64206	0.00075	15.73372	0.00084	38.55766	0.00242	0.80102	0.00001	1.96301	0.00005
βD5r	5	12.296	19.49708	0.00063	15.71689	0.00060	38.60251	0.00162	0.80611	0.00001	1.97993	0.00003
βD8	3	6.966	19.51840	0.00075	15.71837	0.00077	38.58702	0.00226	0.80530	0.00001	1.97702	0.00006
βD12	3	7.536	19.50804	0.00065	15.71636	0.00065	38.58702	0.00185	0.80564	0.00001	1.97802	0.00005
βE1	3	5.807	19.70644	0.00081	15.74395	0.00080	38.55619	0.00251	0.79893	0.00001	1.95653	0.00006
βE4	3	6.786	19.56909	0.00074	15.72375	0.00069	38.56849	0.00230	0.80350	0.00001	1.97088	0.00006
βE7r	5	8.486	19.65747	0.00053	15.73583	0.00054	38.56616	0.00141	0.80050	0.00001	1.96190	0.00003
βE10	3	4.478	20.05535	0.00072	15.78400	0.00073	38.35375	0.00220	0.78701	0.00001	1.91237	0.00005
βE11	3	4.350	19.73946	0.00073	15.74388	0.00079	38.41423	0.00214	0.79759	0.00001	1.94609	0.00006
βE12	3	3.815	19.92735	0.00077	15.76657	0.00077	38.35911	0.00240	0.79120	0.00001	1.92493	0.00005
βE14r	5	6.625	19.92263	0.00062	15.76754	0.00057	38.39399	0.00163	0.79143	0.00001	1.92715	0.00003
Replicates (re-sampled)												
βB9b	4	5.509	19.61541	0.00064	15.72982	0.00068	38.52640	0.00200	0.80189	0.00001	1.96408	0.00005
βC4r	5	10.511	19.60573	0.00058	15.73084	0.00050	38.55847	0.00129	0.80236	0.00001	1.96667	0.00003
βD5e	3	7.719	19.50190	0.00080	15.71608	0.00088	38.58890	0.00286	0.80588	0.00002	1.97876	0.00007
βD8bis	3	6.444	19.43235	0.00076	15.70665	0.00085	38.61480	0.00261	0.80829	0.00002	1.98717	0.00007
Duplicates (re-measured)												
βA5rre			19.56918	0.00067	15.72500	0.00062	38.55580	0.00195	0.80357	0.00001	1.97027	0.00005
βD5ere			19.50531	0.00067	15.71853	0.00066	38.59674	0.00193	0.80585	0.00001	1.97877	0.00004
βD5rre			19.49741	0.00046	15.71741	0.00046	38.60477	0.00144	0.80612	0.00001	1.97998	0.00004
Detrital												
βA5	2	6.728	19.02171	0.00087	15.64317	0.00091	38.89918	0.00282	0.82237	0.00001	2.04493	0.00005
βB3	3	6.341	19.12896	0.00073	15.65673	0.00082	38.78657	0.00264	0.81849	0.00002	2.02764	0.00007
βB6	3	5.777	19.19508	0.00066	15.66468	0.00065	38.84223	0.00207	0.81608	0.00001	2.02355	0.00006
βB9	4	4.821	19.21482	0.00064	15.67725	0.00058	38.83813	0.00176	0.81537	0.00001	2.02125	0.00004

Table 3a (continued)

ID	Session No	[Pb] µg/g	DEPTH (cm)	206Pb/204Pb	2SE	207Pb/204Pb	2SE	208Pb/204Pb	2SE	207Pb/206Pb	2SE	208Pb/206Pb	2SE
βB12	3	6.424	126	19.18696	0.00072	15.66147	0.00076	38.81456	0.00220	0.81626	0.00001	2.02296	0.00005
βB15	3	5.876	144	19.19349	0.00075	15.66857	0.00081	38.83444	0.00258	0.81634	0.00001	2.02330	0.00007
βC1	2	5.909	161	19.08192	0.00069	15.65272	0.00086	38.93244	0.00274	0.82029	0.00002	2.04028	0.00007
βC4	3	5.490	179	19.21777	0.00057	15.67015	0.00069	38.83270	0.00214	0.81540	0.00001	2.02068	0.00006
βC7	3	6.643	197	19.18655	0.00073	15.66329	0.00076	38.79822	0.00226	0.81637	0.00001	2.02214	0.00006
βC10	2	4.998	215	19.04650	0.00080	15.64976	0.00081	38.89747	0.00226	0.82166	0.00001	2.04223	0.00006
βC14	3	6.682	239	19.22782	0.00067	15.67227	0.00072	38.84252	0.00228	0.81508	0.00001	2.02013	0.00006
βD1	3	5.939	257	19.23351	0.00102	15.67282	0.00101	38.83876	0.00304	0.81488	0.00002	2.01937	0.00007
βD5e	4	5.521	281	19.21776	0.00080	15.67051	0.00077	38.85639	0.00236	0.81543	0.00001	2.02193	0.00005
βD8	3	5.007	299	19.21813	0.00078	15.67242	0.00087	38.85785	0.00267	0.81551	0.00001	2.02195	0.00007
βD12	3	6.143	323	19.13760	0.00074	15.65805	0.00076	38.77635	0.00230	0.81818	0.00001	2.02621	0.00005
βD15	2	4.328	341	19.07711	0.00075	15.65438	0.00079	38.94133	0.00232	0.82058	0.00001	2.04126	0.00006
βE1	3	5.989	359	19.12863	0.00080	15.65589	0.00084	38.68113	0.00248	0.81846	0.00001	2.02215	0.00005
βE4	3	6.312	377	19.16417	0.00080	15.65953	0.00083	38.79899	0.00257	0.81713	0.00001	2.02461	0.00006
βE7	2	5.854	395	19.04530	0.00066	15.64806	0.00074	38.91340	0.00227	0.82162	0.00001	2.04320	0.00006
βE10	4	5.125	413	18.78187	0.00067	15.59245	0.00071	38.32156	0.00210	0.83018	0.00001	2.04034	0.00007
βE11	4	5.156	419	18.80898	0.00059	15.60145	0.00065	38.37958	0.00220	0.82946	0.00001	2.04049	0.00006
βE12	4	4.574	425	18.59446	0.00068	15.56797	0.00073	38.17981	0.00228	0.83724	0.00001	2.05329	0.00006
βE14	4	4.195	437	18.63736	0.00070	15.57782	0.00080	38.31511	0.00225	0.83584	0.00001	2.05581	0.00005
Replicates (re-sampled)													
bD8bis	4	3.687	299	19.20611	0.00058	15.67243	0.00064	38.85699	0.00217	0.81601	0.00001	2.02315	0.00005
JC106_151VC													
Leachate													
γB1	1	6.795	98	19.52751	0.00129	15.72978	0.00146	38.56108	0.00493	0.80552	0.00003	1.97472	0.00014
γB6	1	7.369	128	19.46827	0.00081	15.71900	0.00078	38.54373	0.00270	0.80742	0.00001	1.97983	0.00007
γC3	1	6.889	158	19.43074	0.00067	15.71521	0.00067	38.56170	0.00244	0.80877	0.00001	1.98456	0.00007
γC8	1	7.536	188	19.46201	0.00067	15.71914	0.00066	38.54541	0.00225	0.80770	0.00001	1.98050	0.00007
γC13	1	7.308	218	19.33487	0.00054	15.70149	0.00056	38.60225	0.00243	0.81207	0.00001	1.99650	0.00007
γD4	1	7.216	248	19.42019	0.00064	15.71395	0.00068	38.58108	0.00221	0.80916	0.00001	1.98667	0.00007
γD9	1	7.555	278	19.41312	0.00077	15.71402	0.00074	38.57862	0.00265	0.80945	0.00001	1.98727	0.00005
γD14	1	5.666	308	19.41346	0.00076	15.71438	0.00070	38.58059	0.00227	0.80946	0.00001	1.98731	0.00007
γE4	1	5.226	338	19.37582	0.00063	15.70624	0.00062	38.56444	0.00205	0.81061	0.00001	1.99034	0.00006
γE9	1	5.699	368	19.46171	0.00093	15.71884	0.00084	38.53422	0.00259	0.80769	0.00001	1.98002	0.00006
γE14	1	5.985	398	19.39951	0.00055	15.71177	0.00056	38.55583	0.00206	0.80991	0.00001	1.98748	0.00006
Replicates (re-sampled)													
γC3bis	1		158	19.37589	0.00076	15.70703	0.00071	38.58576	0.00211	0.81063	0.00001	1.99135	0.00006
Detrital													
γB1	2	2.272	98	19.23166	0.00084	15.67142	0.00092	38.91801	0.00282	0.81487	0.00002	2.02363	0.00007
γB6	2	2.938	128	19.18099	0.00095	15.66386	0.00100	38.88257	0.00316	0.81663	0.00002	2.02714	0.00007
γC3	4	2.154	158	19.23567	0.00080	15.66927	0.00095	38.88919	0.00282	0.81459	0.00001	2.02168	0.00007
γC8	2	3.062	188	19.21355	0.00069	15.66760	0.00076	38.89141	0.00238	0.81545	0.00002	2.02418	0.00007
γC13	2	2.262	218	19.19249	0.00167	15.66575	0.00192	38.90280	0.00633	0.81624	0.00003	2.02698	0.00016
γD4	2	3.091	248	19.19715	0.00072	15.66897	0.00085	38.90912	0.00245	0.81621	0.00002	2.02683	0.00006
γD9	2	2.427	278	19.19803	0.00079	15.67044	0.00092	38.90089	0.00295	0.81625	0.00002	2.02628	0.00008
γD14	2	3.438	308	18.92866	0.00087	15.62770	0.00100	38.71561	0.00297	0.82561	0.00002	2.04537	0.00007
γE4	2	3.038	338	19.07443	0.00079	15.64854	0.00087	38.83539	0.00278	0.82040	0.00002	2.03600	0.00008
γE9	2	2.845	368	19.10985	0.00096	15.65324	0.00100	38.83093	0.00308	0.81912	0.00002	2.03200	0.00007
γE14	4	2.340	398	18.99362	0.00063	15.63844	0.00076	38.80738	0.00225	0.82335	0.00001	2.04317	0.00006

Table 3b
The average Pb isotope ratios measured on NBS 981 and the optimised $^{205}Tl/^{203}Tl$ ratio used for mass bias correction in each analytical session.

Session no.	Date	Number of standard runs	$^{206}Pb/^{204}Pb$	2SD	$^{207}Pb/^{204}Pb$	2SD	$^{208}Pb/^{204}Pb$	2SD	$^{207}Pb/^{206}Pb$	2SD	$^{208}Pb/^{206}Pb$	2SD	$^{205}Tl/^{203}Tl$
1	15/05/2015	12	16.9417	± 0.00088	15.5004	± 0.00118	36.7205	± 0.00350	0.9149	± 0.00003	2.1675	± 0.00011	2.3888
2	19/11/2015	12	16.9416	± 0.00063	15.4997	± 0.00064	36.7222	± 0.00168	0.9149	± 0.00002	2.1676	± 0.00005	2.3886
3	23/11/2015	14	16.9415	± 0.00060	15.5002	± 0.00079	36.7235	± 0.00228	0.9149	± 0.00002	2.1677	± 0.00007	2.3887
4	24/11/2015	12	16.9416	± 0.00082	15.4998	± 0.00066	36.7217	± 0.00183	0.9149	± 0.00002	2.1676	± 0.00005	2.3886
5	10/02/2016	11	16.9415	± 0.00061	15.4992	± 0.00070	36.7202	± 0.00227	0.9149	± 0.00003	2.1675	± 0.00010	2.3885

4.1. Analytical methods

4.1.1. Separation of Pb in authigenic and detrital fractions

Bulk marine sediments are composed of distinct fractions: exchangeable, bound to carbonates, bound to organic matter, bound to FeMn oxyhydroxides and a residual (detrital) fraction (Tessier et al., 1979). An average of 100 mg of sediment per sample was decarbonated in 8 mL 0.1 M Na acetate-buffered acetic acid for 24 h. Exchangeable ions were removed by a leach in 8 mL 1 M $MgCl_2$. The samples were solubilised in 8 mL of 50 mM hydroxylamine hydrochloride dissolved in 15% glacial acetic acid over a 3-hour period, during which they were gently agitated. The samples were further centrifuged before transfer of 6 mL of the supernatant (dominated by the FeMn oxyhydroxide fraction, henceforth referred to as the leachate) to Teflon vials for drying. After extraction of the FeMn oxyhydroxide fraction, the residual (detrital) fraction was reacted in 50 mM HH + 15% acetic acid for a further 24 h to remove all trace of FeMn oxyhydroxides. The organic matter and remaining authigenic phases were destroyed in consecutive treatments with hydrogen peroxide, aqua regia and perchloric acid accompanied by ultrasonication. The remaining silicates were digested in concentrated HF-HNO_3 over a 3-day period in closed Teflon vials.

4.1.2. ICP-MS and MC-ICP-MS analyses

An aliquot of 10% was collected from both the leachate and detrital fractions for major and trace element analysis. Major element analysis was performed at the Scottish Association for Marine Science (SAMS) on a Perkin Elmer Optima DV4300 ICP-OES. Trace metals analysis was performed at SAMS on a Thermo Scientific X-Series (II) quadrupole ICP-MS.

The Sr, Nd and Pb fractions were all measured for isotope ratios using a Thermo Fisher Scientific Neptune MC-ICP-MS in the Department of Earth Sciences at Durham University. The basic analytical method used for each element on the Neptune comprises a static multi-collection routine of 1 block of 50 cycles with an integration time of 4 s per cycle; total analysis time ~3.5 min.

The Pb was purified at Durham using Sr-spec resin as described in Font et al. (2008). Prior to analysis, the Pb beam intensity for each sample was tested and spiked with Tl to a constant Pb/Tl ratio. The method applied in this study is presented in the Supplementary Materials. The Pb samples were analysed during six analytical sessions. The optimised $^{205}Tl/^{203}Tl$ ratio used for mass bias correction and the average Pb isotope ratios measured on NBS 981 in each analytical session are reported in Table 3b.

4.1.3. Nd and Sr analysis in the detrital fraction

The Nd and Sr samples were leached in 6 M HCl at 60 °C in an ultrasound for 30 min and then dissolved with 29 M HF and 16 M HNO_3 (3:1). The dissolution and column procedures for the separation of Sr from whole-rock matrices are described in Font et al. (2008). For Sr isotope ratio measurements instrumental mass bias was corrected for using a $^{88}Sr/^{86}Sr$ ratio of 8.375209 (the reciprocal of the $^{86}Sr/^{88}Sr$ ratio of 0.1194) and an exponential law. Samples were analysed during one analytical session during which the average $^{87}Sr/^{86}Sr$ value for NBS987 was 0.710271 ± 0.000012 (16.5 ppm; $n = 7$). Sr isotope data for samples is normalised to an accepted NBS987 value of 0.71024 Thirlwall (1991).

For Nd isotope ratio measurements instrumental mass bias was corrected for using a $^{146}Nd/^{145}Nd$ ratio of 2.079143 (equivalent to the more commonly used $^{146}Nd/^{144}Nd$ ratio of 0.7219) and an exponential law. $^{146}Nd/^{145}Nd$ are used for mass bias correction since Nd is analysed as part of a total rare earth element (REE) column cut and they are the only two REE interference-free Nd isotopes. Samples were analysed during a single analytical session during which the average $^{143}Nd/^{144}Nd$ value for pure and Sm-doped JNDi-1 standards was 0.512094 ± 0.000009 (17 ppm 2SD; $n = 9$). Samples were analysed during a single analytical session during which the average
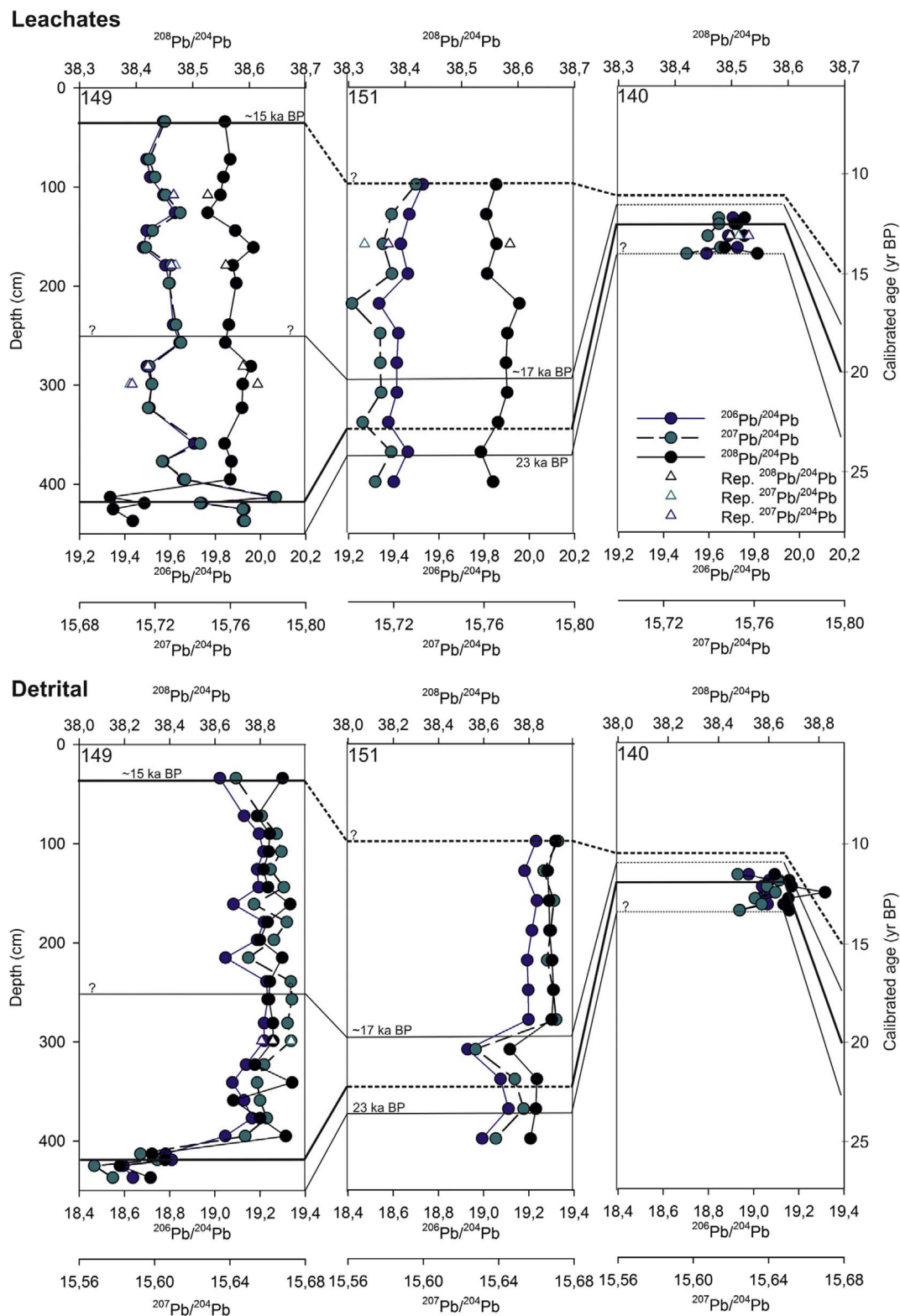
Fig. 3. Pb isotope ratios for the leachate (top) and detrital (bottom) fraction of the three cores plotted against depth. Age intervals calculated from the age models are also presented. Replicates for same sample depth are shown with triangles (see legend).

$^{143}Nd/^{144}Nd$ value for pure and Sm-doped JNdi-1 standards was 0.512094 ± 0.000009 (17 ppm 2SD; n = 9). Nd isotope data for samples are reported relative to a JNdi value of 0.512115 equivalent to a La Jolla value of 0.511858 Tanaka et al. (2000).

The Supplementary material details in full all procedures relating to column chromatographic separation procedures for Pb, Sr and Nd,

major and trace elements analysis and mass spectrometry, including reproducibility of the leaching approach.

4.2. Chronostratigraphy

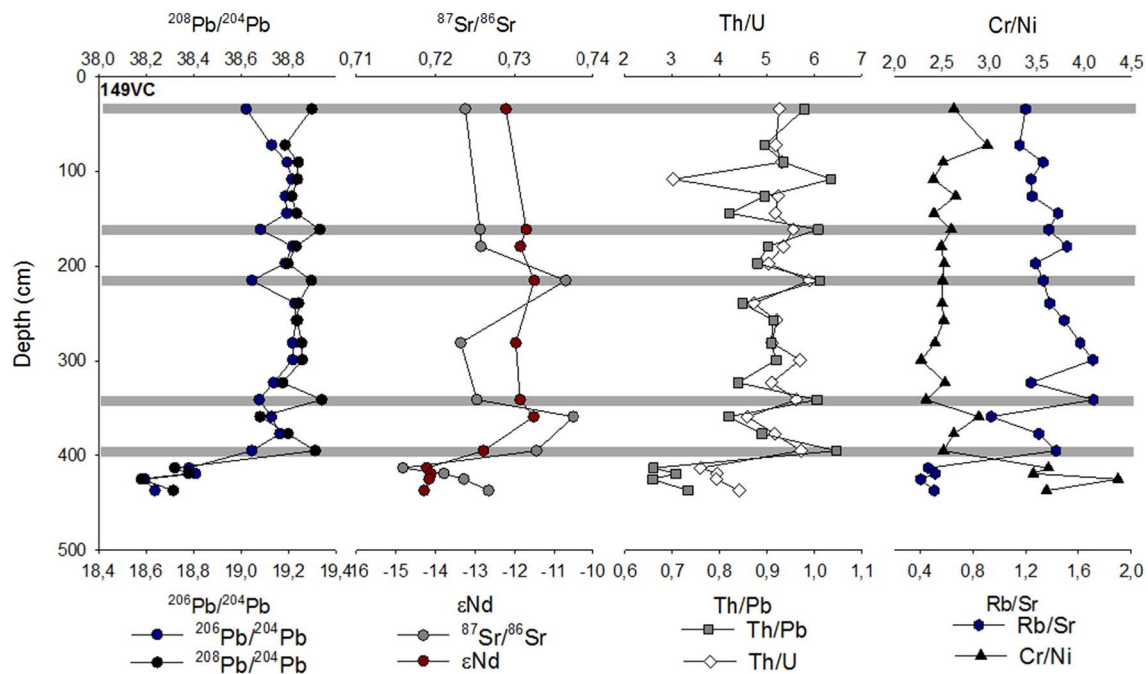Bivalve shells (whole valves and fragments) were sampled and

Fig. 4. $^{206}Pb/^{204}Pb$, $^{208}Pb/^{204}Pb$, $^{87}Sr/^{86}Sr$ and εNd with Th/U, Th/Pb, Rb/Sr and Cr/Ni ratios (g/g) of the detrital fraction in core 149, all plotted against depth. In grey are highlighted the spikes in $^{208}Pb/^{204}Pb$ (see text).

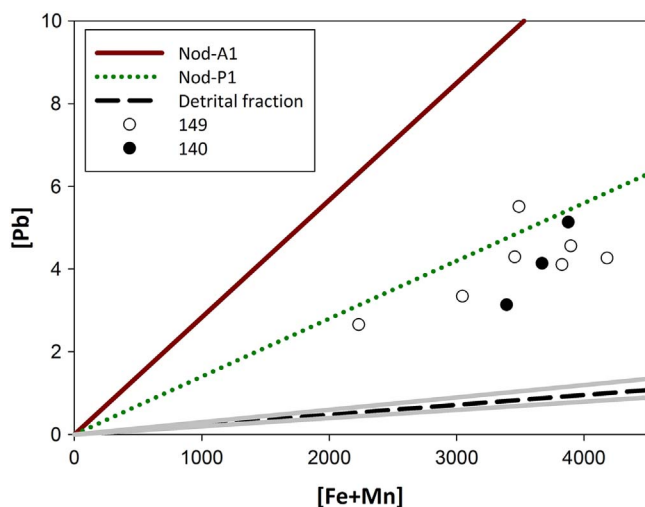**Fig. 5.** Concentration of Pb and combined Fe + Mn from the leached fraction of cores 140 and 149. The lines denote the [Pb]/[Fe + Mn] ratios of bulk FeMn nodules from the North Atlantic (Nod-A1), Pacific (Nod-P1) (Axelsson et al., 2002), and the detrital fraction of the two cores with the 1SD envelope. The errors on the leachates are smaller than the symbols on the plot.

dated in order to produce an age model for the cores. The relative scarcity of foraminifera in core 149 prevented monospecific foraminiferal samples being used to provide more ages to constrain the age model. The samples were sent to [14]CHRONO Centre in Queen's University Belfast, NERC Radiocarbon Facility in East Kilbride and the Radiocarbon laboratory at University of California for radiocarbon dating.

Nine ^{14}C accelerator mass spectrometry (AMS) radiocarbon dates were obtained from the three cores (Table 2). Dates were calibrated into calendar ages using Calib v7.1 (Stuiver et al., 2016) with the MARINE13 calibration curve (no deltaR applied, Reimer et al., 2013). The paucity of dated material does not permit the production of a robust age model for the three cores, nevertheless the constraints permit a correlation of the different sections analysed. The laminated muds in

core 149 extend from a maximum age of 20.1 cal ka BP at the diamicton-laminated mud interface to a maximum of 14.8 cal ka BP at the top of the laminated muds. The date of 10.8 cal ka BP in the upper mud unit is interpreted as spurious, produced by bioturbation. Potential hiatuses or internal changes in the sedimentation rates are not readily identifiable. However, the extremely delicate lamination in this unit (visible on X-ray scans, Fig. 2) supports consistency in sedimentation rate, suggesting a low-energy environment, with sedimentation under a seasonal or even diurnal influence related to tidal activity (cf. Dowdeswell et al., 2000), which is known to have been prominent in the area after the LGM (Uehara et al., 2006). An age of 10.3 ± 0.13, obtained from a small bivalve fragment at 2.2 m is interpreted as spurious, as too young to belong to glacimarine sediments. The fragment was probably moved in the core cutting process. In core 151 two dates of ~16.8 and 23.2 cal ka BP constrain the time of deposition of the lower part of the core, and indicate a correspondence to part of core 149. The middle part of the iceberg-turbated diamicton in core 140 is dated at 21.5 cal ka BP, and its deposition probably ceased well before 12.1 cal ka BP (obtained at 0.96 m in the upper sandy mud unit). A maximum age of 50.7 ± 2.5 ka BP was obtained at 2.99 m core depth, indicating that the second diamicton unit is most likely a pre-Late Devensian glacimarine deposit, overridden and compacted at LGM. The sampling has therefore been restricted to the top diamicton unit.

5. Results

The Pb isotope results are presented in Tables 3a and 3b; the Sr and Nd isotope data, and major and trace element concentrations are provided in the Supplementary material.

5.1. Pb in leachates

In cores 140 and 151 the ranges in Pb isotope ratios are relatively small, while core 149 presents the most variable Pb record (Fig. 3). The $^{206}Pb/^{204}Pb$ varies between 19.59 and 19.79 in core 140, compared to 19.34 and 19.51 in core 151. The $^{207}Pb/^{204}Pb$ ratio instead varies from 15.73 to 15.74 in core 140, and 15.70 to 15.73 in core 151. Of these two, core 140 displays the most radiogenic isotope ratios, and core 151
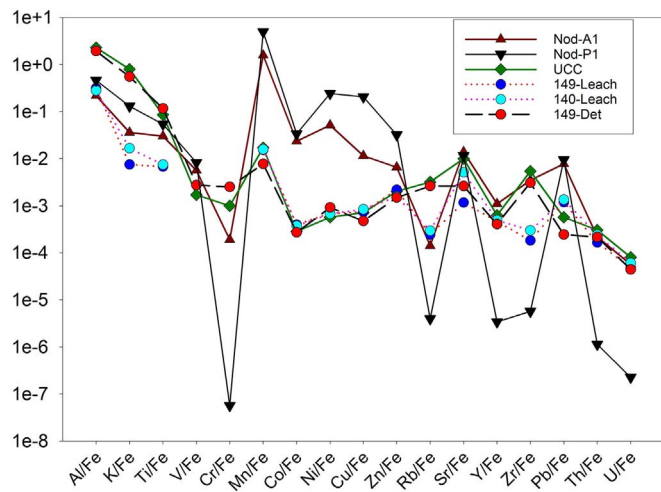
Fig. 6. Element/Fe ratios (g/g) plotted for the leachates and detrital fractions in cores 140 and 149 in comparison to Nod-A1 and P1 values (Axelsson et al., 2002) and upper continental crust (UCC) values (Taylor and McLennan, 1995).
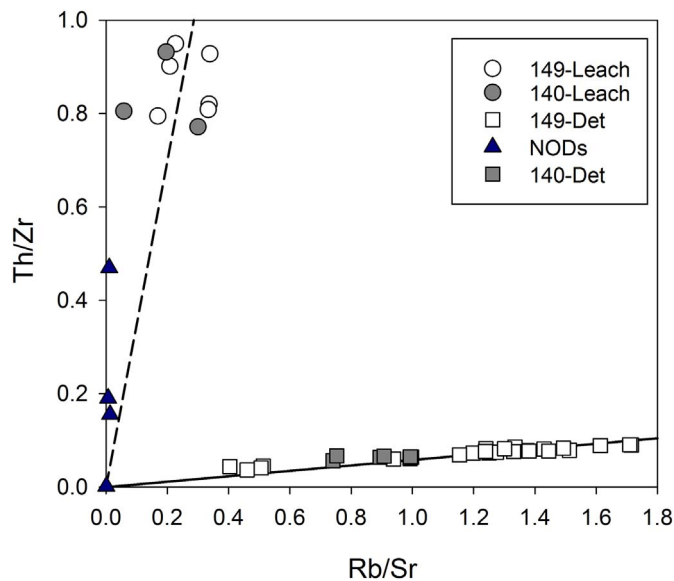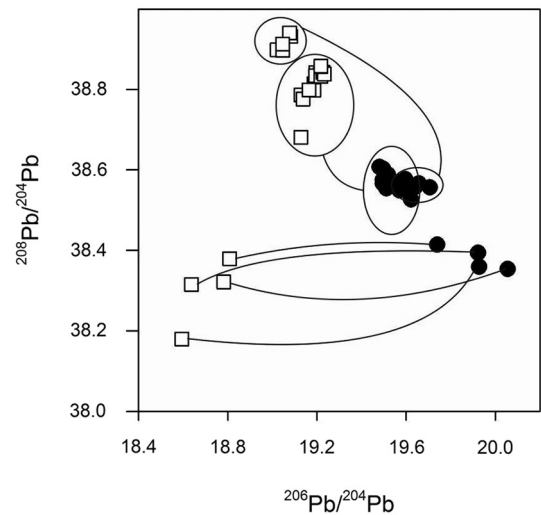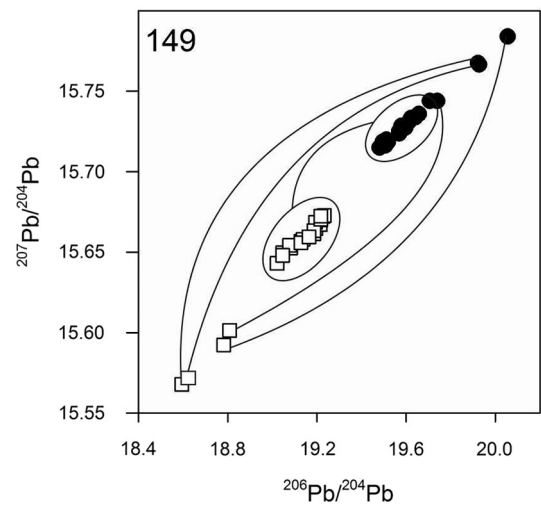

Fig. 7. The detrital fraction and leachates for cores 140 and 149 plotted alongside Nod-A1 and Nod-P1 (NODs) values on Rb/Sr vs Th/Zr space. Regression lines are forced through the origin.

Fig. 8. $^{207}Pb/^{204}Pb$ and $^{208}Pb/^{204}Pb$ vs $^{206}Pb/^{204}Pb$ of the leachate and detrital fractions in core 149. Correspondence between sample or sample group is provided.

presents the most unradiogenic ratios of the three records. The ratios follow a pronounced excursion from higher $^{206}Pb/^{204}Pb$ (up to 20.05) and $^{207}Pb/^{204}Pb$ ratio (~15.79) in the diamicton to a less radiogenic signal (19.48 and 15.71 respectively) in the glacimarine sequence that is from older to younger sediments. A completely different behaviour is observed in all the three cores in $^{208}Pb/^{204}Pb$ ratios, which evolve in a mirror-like fashion in respect to the other two isotope records. In core 149, the $^{208}Pb/^{204}Pb$ values increase from ~38.35 to 38.55 in the lower part and then oscillate in a roughly reversed way to the other two Pb isotope ratios, with peaks corresponding to troughs in $^{206}Pb/^{204}Pb$ and $^{207}Pb/^{204}Pb$ values and vice-versa. The same is observed in core 140, while core 151 presents prominent inversions only at 368 cm and in the interval between 218 and 128 cm.

5.2. Pb, Sr and Nd in detrital fraction

Pb isotope ratios for the residues are generally lower than the corresponding leachates (Crocket et al., 2013; Gutjahr et al., 2009; Kurzweil et al., 2010). In both cores 149 and 151 there is a pronounced

decrease of Pb ratios towards less radiogenic values at respectively 377 cm and 278 cm downcore. In core 149, where it corresponds to the change from glacimarine mud to diamicton, Pb ratios decrease from about 19.24 to 18.9 ($^{206}Pb/^{204}Pb$). Core 151 presents in general higher Pb ratios than core 149, and the excursion is less pronounced (Fig. 3). A similar trend is observed for the $^{87}Sr/^{86}Sr$ ratios in core 149, with values between 0.7185 and 0.7194 in the diamicton, and between 0.726 and 0.7324 in the upper section. The Nd isotopic composition is generally low, with εNd ranging from −14.85 to −10.5, and it does not show consistent trends or variations along the core.

The glaciarmarine muds in core 149 show little variation, with values of $^{206}Pb/^{204}Pb$ between 19.1 and 19.2 along the whole record. Five spikes in $^{208}Pb/^{204}Pb$ correspond to a decrease in both $^{206}Pb/^{204}Pb$ and $^{207}Pb/^{204}Pb$ values. These peaks correspond also to an increase in Th/U and Th/Pb ratios (Fig. 4) and are not related to IRD-rich intervals (Fig. 2). Equivalent features are not observed in core 151.

5.2.1. Grain size and isotope ratios

For this study bulk sediment analyses were preferred, contrary to single-grain provenance studies, (e.g. Colville et al., 2011; Fagel et al.,
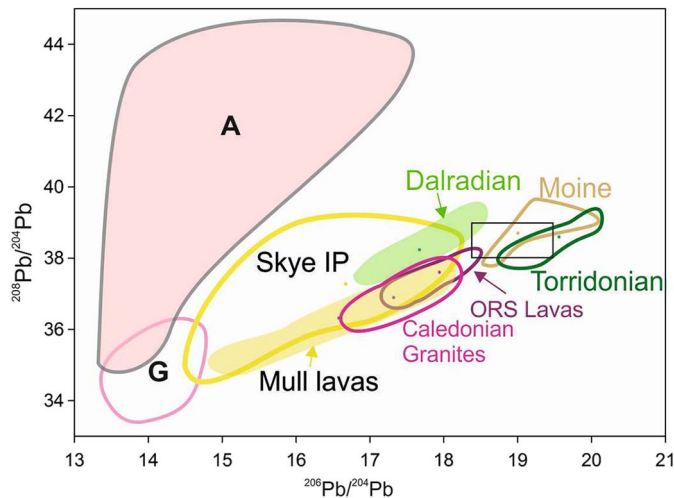
Fig. 9. Fields of potential source areas plotted in Pb/Pb space. Data are from the following sources. Lewisian basement (A = amphibolites; G = granulites): (Dickin and Jones, 1983; Floyd et al., 1989; Hamilton et al., 1979; Kerr et al., 1995; Moorbath et al., 1969, 1975; Muir et al., 1993; Weaver and Tarney, 1980). Torridonian sandstones: (Dickin and Exley, 1981; Dickin and Jones, 1983). Moine metasediments (Geldmacher et al., 1998, 2002; Lambert et al., 1981; Preston et al., 1998). Dalradian metasediments (Dickin et al., 1981; Frost and O'Nions, 1985; Lambert et al., 1982; Van De Kamp, 1970). Caledonian granites and Lorn lavas (Blaxland et al., 1979; Clayburn, 1988; Clayburn et al., 1983; Frost and O'Nions, 1985; Johnstone et al., 1979; Thirlwall, 1982, 1986). British Tertiary Igneous Province (Bell et al., 1994; Dickin, 1981; Dickin et al., 1984; Dickin and Exley, 1981; Geldmacher et al., 2002; Gibson, 1990; Kerr et al., 1995; Moorbath et al., 1969; Preston et al., 1998). Average values and standard deviations are shown in Table A2.9, in the Supplementary Materials. The small box indicates the position of Fig. 10.
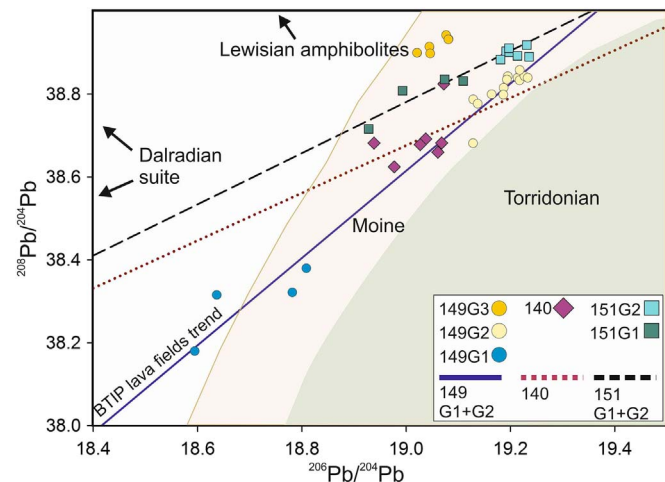

Fig. 10. The $^{208}Pb/^{204}Pb$ vs. $^{206}Pb/^{204}Pb$ of the detrital fraction from the three cores and regression lines for each. Sediment source domains are also indicated. Core 149 is divided in the three groups (G1, G2 and G3) described in the text. Core 151 is divided in G1 and G2. The R^2 values for the regression lines are: 0.97 (149G1 + G2), 0.91 (151G1 + G2) and 0.21 (140).

2002; Farmer et al., 2003; Small et al., 2013). This is because bulk sediment analyses are more easily compared to the numerous Pb, Sr and Nd bulk analyses of Scottish rocks in the literature, and also to avoid potential problems with the leaching procedure (i.e. avoid sample contamination produced by sieving). Nonetheless, the < 125 μm fraction constitutes the majority of all the samples (about ∼ 97–98% weight). As described above, in core 149 the sharp decrease in detrital Pb isotope ratios is also closely associated with the transition to the diamicton, with the matrix composed of 60–70% of particles < 125 μm. While in this case it is conceivable that the different granulometry affected the isotope ratios, the following points should be made before drawing final conclusions:

- The relation between grain size in the sediment and the lithology of the source rocks is not well established and other studies (e.g. Farmer et al., 2003) have shown how different fractions do not necessarily produce different isotope ratios. This is also supported by the decade-long use of IRD counting techniques to establish sediment sources, which would be skewed if fine-grained or soft rock sources were not represented in the > 150 μm fraction.
- At 359 cm in core 149 (Fig. 2) a sandy mud interval presents Pb isotope ratios equivalent to the ones of the adjacent clay, suggesting that granulometry in this case does not affect the results in any prominent way.
- The general trend in both cores 151 and 149 indicates a decrease in the Pb isotope ratios towards lower values in the LGM, indicating a change to sediment sources with these lower values.

6. Discussion

6.1. Detrital contribution to leachates

Recent work on testing leaching protocols (cf. Blaser et al., 2016; Du et al., 2016), albeit with some differences to the method in this study, has highlighted the negligible influence of detrital contamination of leachates as an artefact of laboratory processing. However, assessing detrital contamination of the leachates is an issue that must be considered (Crocket et al., 2012, 2013). A first approach to check for detrital contamination is proposed by Bayon et al. (2002). Since Ti concentrations in seawater and biogenic material are very low, it is assumed that Ti contents measured in leachates are derived exclusively from contamination by terrigenous (detrital) material during the leach with the hydroxylamine hydrochloride solution. The concentrations of Ti in the samples are barely detectable (< 26 ppm) compared to upper continental crust (UCC) values (∼ 0.3 wt%, Taylor and McLennan, 1995), suggesting that no significant detrital contamination has occurred during the leach. Also the Ti/Fe ratio is one order of magnitude lower (∼ 0.0075 Ti/Fe) compared to typical UCC material (0.08 Ti/Fe; see Supplementary material). A second test, proposed by Crocket et al. (2012) uses the concentrations of Pb vs Fe + Mn for the oxyhydroxide fraction (Fig. 5), comparing them to the trends observed in bulk samples of FeMn nodules Nod-A1 and Nod-P1 (Axelsson et al., 2002), from the Atlantic and Pacific Oceans respectively, and the trend outlined by the measured detrital fraction. The majority of leachates plot close to the trend of the Nod-P1, representing [Pb]/[Mn + Fe] ratios derived solely by precipitation of Fe rich phases from seawater. The caveat here is that the mineral phases in the leachate samples are not necessarily the same as those in FeMn nodules, and therefore the solution-mineral
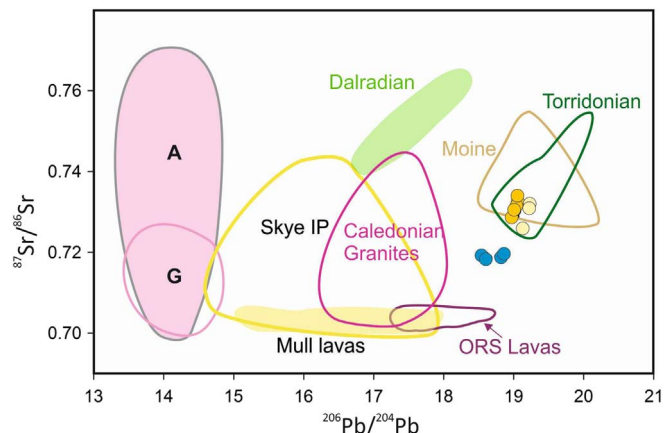

Fig. 11. Detrital $^{87}Sr/^{86}Sr$ vs. $^{206}Pb/^{204}Pb$ of samples from core 149 (small circles; respectively G1 in blue, G2 in beige and G3 in orange) against western Scottish sources. (For interpretation of the references to colour in this figure legend, the reader is referred to the web version of this article.)

partitioning behaviour of trace metals may be slightly different, with implications for the trace metal ratios incorporated in the FeMn oxyhydroxide phases leached in our study.

6.2. Influence of proximity to the ice margin on FeMn oxyhydroxide composition

In order to interpret the significance of the Pb ratios it is necessary to identify the origin of the FeMn oxyhydroxides, that is whether they are allochthonous, i.e. formed in a continental setting ("pre-formed"), or autochthonous, formed from dissolved constituents in a marine settings. Pre-formed FeMn oxyhydroxides precipitate in response to chemical weathering in a variety of environments, including the subglacial (Raiswell et al., 2006), and are likely to have different trace metal compositions from marine authigenic precipitates (e.g. FeMn crusts and nodules), reflecting the range of concentrations of trace metals present in the solutions from which they precipitate. They are also likely to have precipitated under different Eh-pH conditions, thus preserving the

evidence of distinctive solid-solution partitioning behaviour compared to that typically occurring in seawater.

To investigate the origin of the FeMn oxyhydroxides, comparisons of typical concentrations in uniquely marine precipitated FeMn nodules to the leachate samples in this study can be made in order to help ascertain the origin of the FeMn oxyhydroxide precipitates, the idea being that similar patterns of relative element abundance indicate a similar environment of precipitation. One caveat is that marine FeMn nodules may not have exactly the same phases as extracted in the leachates. Ferromanganese nodules contain variable proportions of vernadite, amorphous Fe oxyhydroxides and aluminosilicate minerals (Hein et al., 1996), whereas the leachates are thought to be almost exclusively FeMn oxyhydroxides. At least the leaching reagents target only the most labile FeMn phases dominated by ferrihydrite and lepidocrocite; (Poulton and Canfield, 2005).

In Fig. 6 the average leachate metal/Fe ratios for cores 149 and 140 are plotted alongside values for Nod-A1, Nod-P1, the average upper continental crust (UCC, Taylor and McLennan, 1995) and the detrital
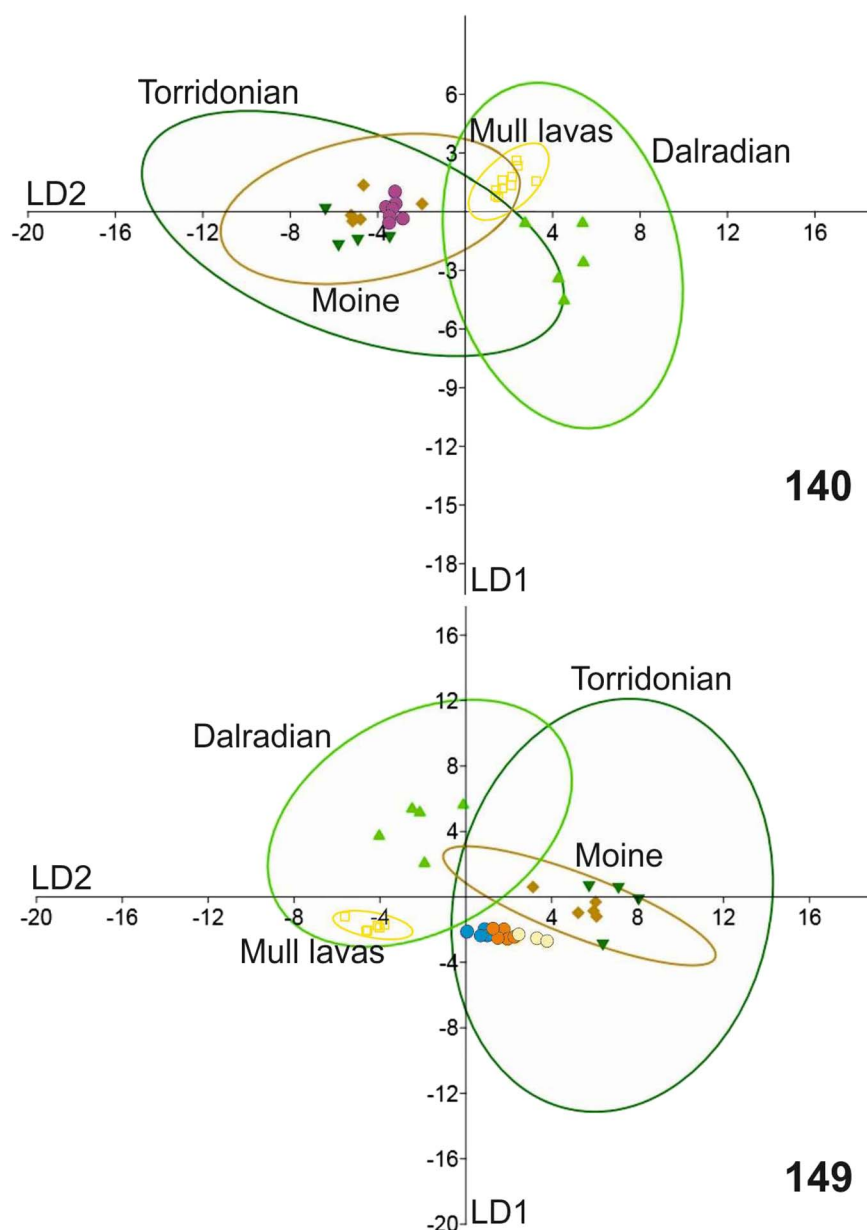

Fig. 12. Linear discrimination analysis (LDA) results of detrital fractions for cores 140 (top panel) and 149 (bottom panel). Core 149 is divided in the three groups (G1, G2 and G3) described in the text.
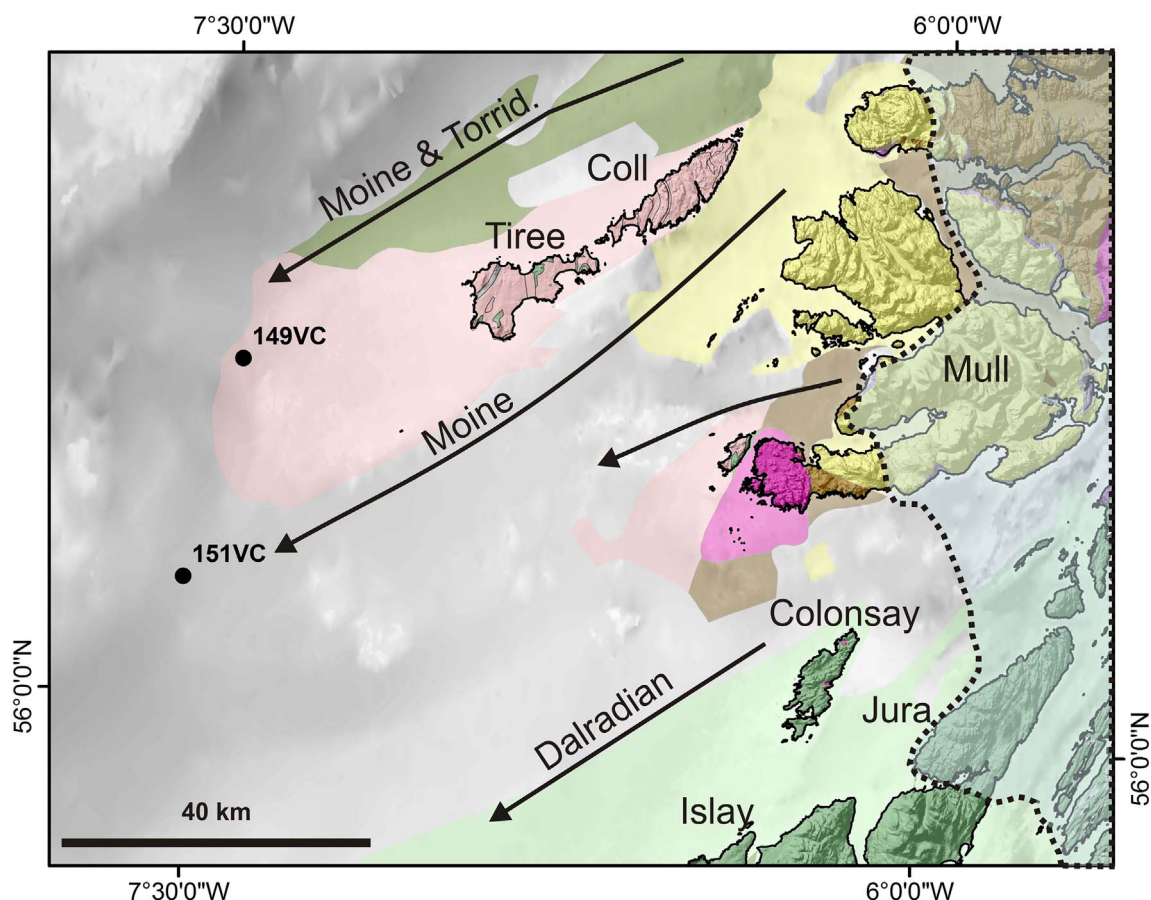
Fig. 13. Inferred ice margin position at ~16.5 ka (Small et al., 2017) and major source pathways reconstructed from this study. The key to lithology types is given in Fig. 1.

fraction in core 149. A ratio to Fe was chosen because iron is the dominant matrix element in FeMn oxyhydroxides and also a major component of rocks. Here the transition metals (Cr, Mn, Co, Ni, Cu, Zn) show the greatest divergence between marine authigenic deposits and crustal material, which suggests they form a good basis for discriminating between a terrigenous and marine origin of the leachates in this study. However, the trend of the leachates for these metals is strikingly similar to UCC and the detrital fraction values, suggesting the FeMn oxyhydroxides in cores 149 and 140 precipitated in a non-marine environment.

While the transition metals point to a terrigenous origin of these FeMn oxyhydroxides, other aspects of their composition highlight the distinctly non-detrital nature of these leachates. A plot of Th/Zr vs. Rb/Sr ratios (Fig. 7) clearly shows the marked difference between the leachates and both the detrital fraction and marine FeMn nodules, suggesting again absence of laboratory detrital contamination but a geochemical signature not attributable to a marine environment. The source of elevated Th/Zr could result from FeMn oxyhydroxide precipitation in or proximal to the subglacial environment. High Th concentrations are expected in waters where sources of Th are abundant, for example in subglacial to proglacial environments. In addition, its significantly greater particle reactivity relative to Zr, reflected by the disparity in marine residence times of 45 years and 5600 years respectively (Johnson et al., 2016), could account for the observed Th/Zr ratios in the leachates. The lower Rb/Sr ratios observed in the leachates compared to the detrital fraction could be due to the effects of glacial erosion and weathering. Glacial sediments are known to preferentially release radiogenic Sr (Blum and Erel, 1995) most likely from high-Rb sheet silicates such as biotite (Blum et al., 1993). This process also influences the concentration of Sr released into solution, especially when water fluxes (or melting of the ice sheet) are high (Anderson et al., 1997; Buggle et al., 2011).

Subglacial FeMn oxyhydroxides are dominated by ferrihydrite, lepidocrocite and nanoparticulate goethite (Poulton and Canfield, 2005; Raiswell et al., 2006), although more extreme conditions can result in precipitation of phases such as schwertmannite and indicate a precipitation environment with low pH (Raiswell et al., 2009). The nanoparticulate phases are highly reactive in the marine environment (Raiswell, 2011), although the proximity of the cores to land reduces the possibility of dissolution before deposition. From these results it is possible to conclude that the FeMn oxyhydroxides are not marine in origin, they have not been influenced by laboratory artefacts, but they do show chemical trends (elevated Th/Zr, low Rb/Sr) that are suggestive of formation in subglacial to proglacial environments.

Further insights into the nature of the FeMn oxyhydroxides on the Malin shelf is given by the marked disassociation in the behaviour of [208]Pb in respect to the other two radiogenic isotopes, observed in all the cores in the Malin Sea. As shown before, the [208]Pb signal delineates an inverted pattern and, especially in core 149, it is almost specular to the other two isotope ratios. Moreover, when plotting the FeMn oxyhydroxide and detrital fraction together, higher [208]Pb/[204]Pb ratios are found in the detrital fraction compared to the leachates (Fig. 8). This second inversion indicates that the bulk sediment cannot account for the leachate composition, as the FeMn precipitates should contain greater quantities of radiogenic Pb (obtained from preferential leaching of radiogenic Pb-rich mineral phases) than the bulk source rock.

The easiest explanation for this atypical behaviour is the presence and interplay of at least two isotopically distinct pools of labile Fe phases carried in weathering fluids of different provenance: WF1, more enriched in thorogenic Pb than the second, WF2. The inversions observed in the record would therefore be caused by variable mixing of the two fluids, with peaks in [208]Pb corresponding to periods of increased influx of WF1 and, vice-versa, troughs when WF1 is prevalent. The two fluids are not easily ascribable to any single lithology in
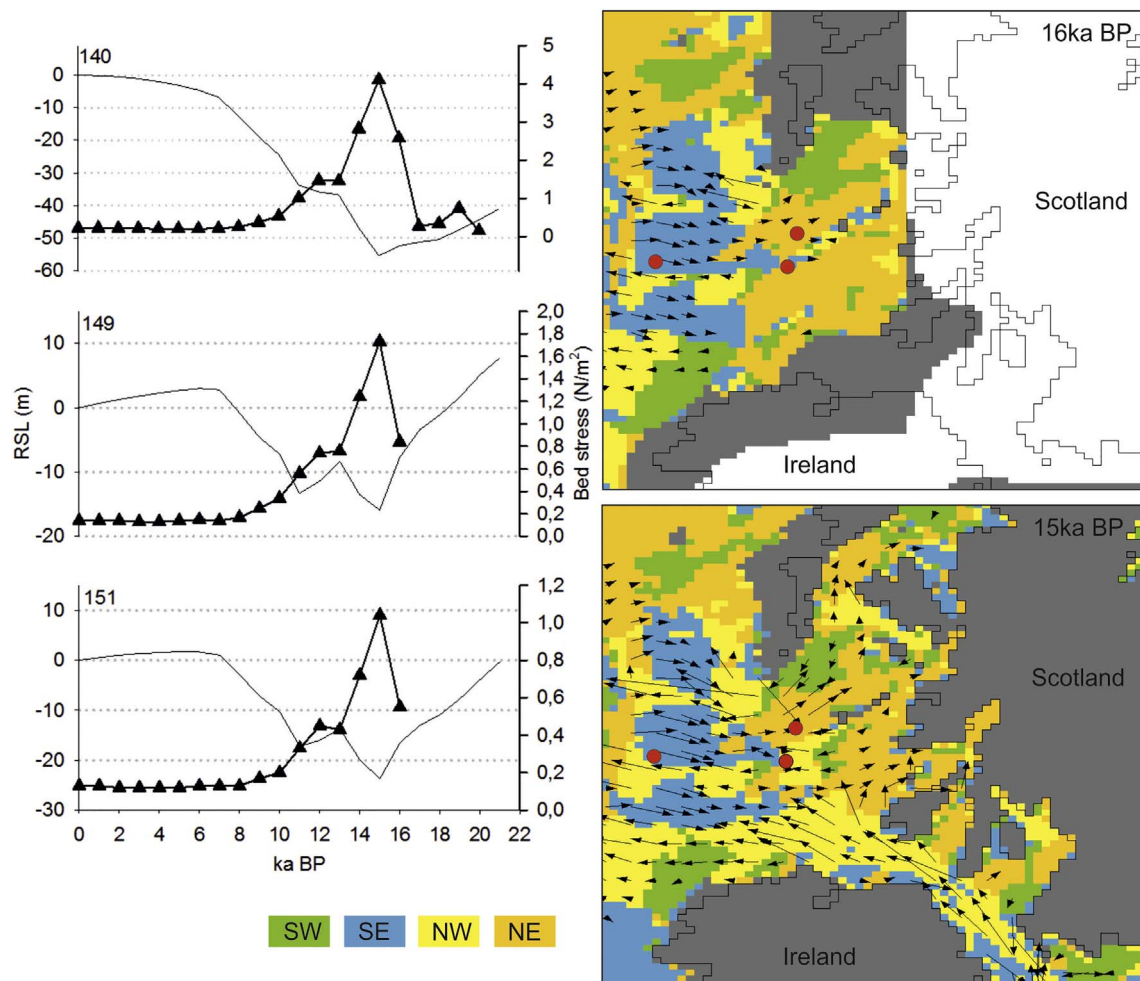
Fig. 14. On the right: visualisations of palaeotidal simulation output based on Ward et al. (2016) using palaeotopography from Bradley et al. (2011). Colours show bed stress vector orientations (orange: NE, green: SW, yellow: NW, blue: SE, see key on figure) with values > 1 N/m² shown with a vector arrow. On the left: relative sea-level curves and bed stress magnitude (triangles) for the core locations produced by the same model. (For interpretation of the references to colour in this figure legend, the reader is referred to the web version of this article.)

western Scotland, but suggest a decoupled behaviour between dissolved Pb and Pb in the suspended clay-silt fraction, probably dictated by the different mobility of the two under the strong tidal regime of the period. A similar conclusion can be drawn by the different variations through time displayed by the two fractions, where trends and peaks do not overlap in a consistent manner.

A tentative comparison of core 149 can be drawn to the one obtained from ODP Site 980 in the Rockall Trough, located West of the Barra-Donegal Fan. Here a sharp decrease in all the three isotope ratios is observed during final retreat of the ice sheet away from the shelf. The $^{206}Pb/^{204}Pb$ decreases from about 21 to 19.5 at about 17.5 ka (Crocket et al., 2013), showing an even more pronounced excursion from LGM to Holocene than the one observed in core 149. The more radiogenic Pb isotope ratios of core 149 could be associated with the proximity of the core to the Scottish ice sheet and therefore the higher intensity and density of the continent-derived labile Fe phases.

The absence of an excursion in core 151, which includes older deposits than core 149 can be associated to the different geographical setting, with core 151 subjected to less terrigenous influence than core 149. This hypothesis is corroborated by the lower abundance of coarse IRD at the bottom of core 151 (Fig. 2), which is the cause of the radiogenic excursion in the other core. Moreover, bioturbation and presence of macrofauna in core 151 indicate that the sediment was probably deposited further away from the ice margin. Unfortunately, absence of trace metal data makes the

assessment of the origin of these oxyhydroxides unfeasible, and a possible up-core switch to dominant marine precipitates cannot be ruled out.

6.3. Sources for the glacimarine sediments

When plotted in Pb/Pb space, the Pb isotopic compositions of the residues from the three cores roughly define linear arrays as shown in Fig. 10. With some differences, the detrital Pb isotope ratios for all the cores and the Sr and Nd ratios for core 149 plot within the range of Moine and Torridonian sediments and are therefore interpreted as derived mainly from erosion of these rock types (Figs. 1 and 9). The Pb isotope ratios in the cores also define trends towards more radiogenic ratios from older to younger sediments, with each trend representing changes of the relative mixing proportions between the dominant Moine-Torridonian and a second (or more) Pb source. The trends for the three cores are plotted in Fig. 10.

Core 140 shows the least variation in Pb isotopes. Unexpectedly, the Pb geochemistry of the detrital fraction is in no perceptible way affected by the characteristically low values of the Lewisian gneisses, the most proximal and extensive rock type present. This signature suggests that either gneisses were not mechanically pulverised and produced mainly coarser sandy fractions (Andrews et al., 1989; Andrews and Principato, 2002; Larsen, 1983), or eroded material was conveyed in a E-W (or northern) direction from the Outer Hebrides at the time. The second hypothesis is supported by seabed stress vectors produced for

the study region by the Bradley-ROMS palaeotidal model (Fig. 14), which indicate prevailing NE-directed stresses.

In core 149, Pb ratios are subdivided into three clearly separated groups that correspond respectively to the diamicton sediments (G1), the bulk of the glacimarine sediments (G2) and the samples with unusually high ^{208}Pb and Th/Pb (G3) described previously. The trends defined by G1 and G2 are the most similar and oscillate between the main Moine-Torridonian source and a second end member, assigned to igneous volcanic rocks. The same trend is observed in the ^{87}Sr/^{86}Sr vs ^{206}Pb/^{204}Pb plot (Fig. 11). Moreover, high Cr/Ni ratios (~4) found in the G2 detrital fraction relative to the two other sample groups (~2.5) are readily correlated to basalts and basaltic andesites on Mull (~4.2) than average Moine sediments (~1.9) (Preston et al., 1998) (Fig. 4). The peaks in ^{208}Pb in core 149 cannot be interpreted as variations within the Moine range as they are too regular in the inversion of the other two Pb ratios and present distinct Th/Pb ratios (Fig. 4). High Th/Pb and ^{208}Pb/^{204}Pb with comparatively lower ^{206}Pb/^{204}Pb are found in both Dalradian and Lewisian rocks, and the distinction between the two cannot be resolved only on a geochemical basis. High Th (and Rb) proportion found in the samples (compared to source rocks) can however be an effect of silicate weathering (e.g. Chen et al., 1999). The strong linear behaviour of Rb/Sr ratios in the detrital fraction of core 149 (Fig. 7) suggests some degree of element fractionation due to clay formation, and therefore isotopic discrimination remains a more reliable way of source discrimination.

Core 151 plots on a different trend shown in Fig. 10. The second end member this time is tentatively assigned to the Dalradian metasediments.

6.3.1. Discriminant function analysis

Although portions of the diagrams discussed above may be provenance distinctive, a considerable degree of overlap exists between Moine and Torridonian rocks, which are more closely related to the values of the samples. In an attempt to improve differentiation between the groups, discriminant function analysis (DFA) has been applied to the data. The object of DFA is to derive a set of linear functions based on multiple variables, designed to achieve best separation between predefined groups of standard data (Klovan and Billings, 1967). The analysis for this work was made using the discriminant procedures available in the free software for statistical computing R (lda function). Taking advantage of the, albeit limited, data present in literature, seven variables have been utilised for DFA: ^{206}Pb/^{204}Pb, ^{207}Pb/^{204}Pb, ^{208}Pb/^{204}Pb, ^{87}Sr/^{86}Sr, ^{143}Nd/^{144}Nd, Th/Pb and Th/Zr.

The results from this exercise are shown in Fig. 12. Three main points can be gathered from the DFA. First of all, in both cores 140 and 149 it was not possible to attain a complete separation of the Moine and Torridonian clusters, however the samples are assigned by the analysis completely to the Moine cluster (minimal Mahalanobis distance). Even more, core 140 plots entirely in the confidence ellipse of the Moine sediments. Secondly, the three groups of core 149 retain evident distinctions; of the three, the average glacimarine sequence (G2) is the most related to the Moine cluster. Thirdly, G1 (blue) and G3 (gold) are statistically close but not within the Moine cluster, supporting the already proposed evidence for other competing sources of those sediments.

6.4. Implications for the retreat of the HIS

The sediment deposited in the three locations encompasses an overall time span between 24 and ~14 cal ka BP. It is possible however that the upper part of core 151 is even younger. In all the locations and through the entire time span the dominant source is that of Moine pelites and psammites from NW Scotland. The only marked exception is the diamicton in core 149 (G1), where the influence of volcanic rocks determines a prominent shift in isotope ratios. Although a clear geochemical distinction between the three different sources of lavas (the

Skye, Mull and Lorn fields) is not possible with the data at our disposal, some speculation can be made in terms of extent and geographical proximity. Firstly, the Mull and Skye lava fields are more extensive and proximal to the cores than the Lorn lavas (Fig. 13). Secondly Dalradian Pb would be expected in the sediment together with the Lorn lavas, as they are found in the same area and are more widespread. For these reasons, it is estimated that the Tertiary lavas are the most likely sources. A simple binary mixing calculation between the average Mull and Skye extrusives and the Moine sediments results in ~20% Pb contribution from the lavas in the diamicton (G1, averages given in Table A2.9, Supplementary material). This shift however is interpreted to have been caused by the contribution of more abundant IRD (>125 μm) in the unit, a conclusion supported by high percentage of basaltic grains in >250 μm fraction found in MD95-2002 (Barra Fan, Knutz et al., 2001) between 20 and 15 ka.

From 24 to 18 cal ka BP ice retreated across the Malin shelf (Scourse et al., 2009; Small et al., 2017) in a predominantly W-E direction (Dove et al., 2015). Pb isotope compositions of the glacimarine sediments in core 140 show that the outer shelf location was mainly influenced by Moine-type material and although the most proximal crustal material is that of the Lewisian basement of the Outer Hebrides, little or no input is observed.

The glacimarine clays in cores 149 and 151 were deposited as the ice margin retreated towards the inner lochs in western Scotland. No major influence of the Lewisian rocks of the islands is observed; this result supports the notion of an ice-free Tiree and Coll around that time, as proposed by Small et al. (2017).

After 18 cal ka BP the ice flow directions from the Grampian Terrane (Dalradian) were along a NE-SW axis and sediment was probably transported preferentially southwestwards (Dove et al., 2015). This culminated before ~15.5 cal ka BP, when ice based on the SW Highlands re-advanced onto the Northern Irish Coast during the East Antrim Coastal Readvance (EACR) (Finlayson et al., 2014; McCabe and Williams, 2012; Small et al., 2017). Ice flow directions could thus explain the absence of a major influence of Dalradian sediments in the two shelf cores.

As the proportion of Moine (NW Highlands) is maintained between 17 and 15 cal ka BP, it can only be inferred that significant inputs of Dalradian sediment did not reach the core locations. As ice retreat was mostly constrained along the Scottish sea lochs, it is possible that shelf currents active at the time (Uehara et al., 2006; Ward et al., 2016) contributed to the sediment delivery direction.

In core 149 the spikes in ^{208}Pb are interpreted tentatively as weak pulses of sediment sourced from the amphibolitic gneisses (Lewisian in age) produced by the shrinking independent ice domes on the Outer Hebrides (Stone and Ballantyne, 2006). The regularity of the pulses across the record suggests discrete purging events. An alternative Dalradian source is considered unlikely, as a similar signature would then be expected in core 151, which is geographically closer than 149 to the Grampian Terrane, but further afield from the Outer Hebrides.

Once again, circulation of coastal and oceanic currents could explain the marked differences between core 149 and 151. The North Atlantic Slope Current encroaches periodically on the Scottish shelf, directed northwards (Inall et al., 2009). If this process was active at the time of deposition it is possible that the Lewisian "inputs" were blocked completely from reaching the southern site of core 151 and reduced at core 149. This interpretation is supported by the palaeotidal simulation for the study area shown in Fig. 14. However, the knowledge of the Scottish shelf circulation is still rudimentary, therefore no definitive connections can be drawn between currents and isotope records.

7. Conclusions

Three cores on the western Scottish shelf were characterised in terms of their Pb isotopic composition in both authigenic and detrital fractions in order to study the retreat dynamics and flow sources of the

Hebrides Ice Stream of the BIIS. The Pb isotope records extracted from the FeMn oxyhydroxide fraction of glacimarine sediments indicate a sharp decrease in radiogenic lead from ~21 ka. This decrease is interpreted to represent the break-up of ice streaming in western Scotland around that time, and the consequent reduced flux of continentally-derived FeMn oxyhydroxides to the continental shelf. Furthermore, the $^{208}Pb/^{204}Pb$ ratio shows an unusual inversion relative to the other radiogenic Pb isotope ratios, and is attributed to the introduction of secondary oxyhydroxide phases from a source with contrasting $^{208}Pb/^{204}Pb$ but similar ^{206}Pb and ^{207}Pb.

The isotopic signature of the detrital fraction in the sediments is used to track the relative contribution between different sources. The Pb, Nd and Sr isotope values indicate that a preponderance of Moine-sourced fine sediments, originated from the NW Highlands, was deposited at the core locations from ~18 to 14 ka, probably dictated by the orientation of ice flow and tidal current directions. The absence of the proximal Lewisian gneiss signature suggests that either gneisses are not easily mechanically pulverised and produce only coarser fractions, or that the prevailing NE-directed palaeo-currents carried the material northwards. The latter interpretation is supported by reconstruction of palaeo-current directions and tides. Coarse grains in a basal diamicton shows instead influence of volcanic-derived material, suggesting, in this case, different provenance for different grain sizes. Periodic spikes in $^{208}Pb/^{204}Pb$ point possibly to pulsed increases from a high Th/U source, identified as the amphibolitic Lewisian basement in the Outer Hebrides.

This study demonstrates how lead isotope analyses on continental shelves can be used to constrain the activity and flow sources of palaeo-ice streams. This kind of data can be useful in future attempts to fingerprint IRD from the deep ocean to ice stream sources. Further studies on chronologically better-constrained cores, applying a suite of clay mineralogy, isotope geochemistry and their relations to different grain-size contributions are necessary to unravel a complete dynamic deglaciation history in western Scotland.

Acknowledgements

Appendix A. Supplementary data

Supplementary data to this article can be found online at https://doi.org/10.1016/j.margeo.2017.08.017.

References

Anderson, S.P., Drever, J.I., Humphrey, N.F., 1997. Chemical weathering in glacial environments. Geology 25, 399–402. http://dx.doi.org/10.1130/0091-7613(1997) 025<0399:CWIGE>2.3.CO.

Andrews, J.T., Principato, S.M., 2002. Grain-size characteristics and provenance of ice-proximal glacial marine sediments. In: Dowdeswell, J.A., Ó Cofaigh, C. (Eds.), Glacier-influenced Sedimentation on High-latitude Continental Margins. Geological Society, London, Special Publicationspp. 305–324.

Andrews, J.T., Syvitski, J.P.M., 1994. Sediment fluxes along high-latitude glaciated continental margins: northeast Canada and eastern Greenland. In: Material Fluxes on the Surface of the Earth, pp. 99–115.

Andrews, J.T., Geirsdóttir, Á., Jennings, A.E., 1989. Late Quaternary spatial and temporal changes in clay- and silt-size mineral assemblages of fiord and shelf cores, western Baffin Bay, northwest North Atlantic. Cont. Shelf Res. 9, 445–463.

Austin, W.E.N., Bard, E., Hunt, J.B., Kroon, D., Peacock, J.D., 1995. The ^{14}C age of the Icelandic Vedde Ash: implications for younger dryas marine reservoir age corrections. Radiocarbon 37, 53–62. http://dx.doi.org/10.2458/azu_js_rc.37.1646.

Axelsson, M.D., Rodushkin, I., Ingri, J., Ohlander, B., 2002. Multielemental analysis of Mn-Fe nodules by ICP-MS: optimisation of analytical method. Analyst 127, 76–82. http://dx.doi.org/10.1039/b105706p.

Bailey, I., Hole, G.M., Foster, G.L., Wilson, P.A., Storey, C.D., Trueman, C.N., Raymo, M.E., 2013. An alternative suggestion for the Pliocene onset of major northern hemisphere glaciation based on the geochemical provenance of North Atlantic Ocean ice-rafted debris. Quat. Sci. Rev. 75, 181–194. http://dx.doi.org/10.1016/j.quascirev.2013.06.004.

Bayon, G., German, C.R., Boella, R.M., Milton, J.A., Taylor, R.N., Nesbitt, R.W., 2002. An improved method for extracting marine sediment fractions and its application to Sr and Nd isotopic analysis. Chem. Geol. 187, 179–199.

Bell, B.R., Claydon, R.V., Rogers, G., 1994. The petrology and geochemistry of cone-sheets from the Cuillin Igneous Complex, Isle of Skye: evidence for combined assimilation and fractional crystallization during lithospheric extension. J. Petrol. 35, 1055–1094.

Benn, D.I., Evans, D.J.A., 2010. Glaciers and Glaciation, 2nd ed. Routledge.

Blaser, P., Lippold, J., Gutjahr, M., Frank, N., Link, J.M., Frank, M., 2016. Extracting foraminiferal seawater Nd isotope signatures from bulk deep sea sediment by chemical leaching. Chem. Geol. 439, 189–204. http://dx.doi.org/10.1016/j.chemgeo.2016.06.024.

Blaxland, A.B., Aftalion, M., van Breemen, O., 1979. Pb isotopic composition of feldspars from Scottish Caledonian Granites, and the nature of the underlying crust. Scott. J. Geol. 15, 139–151. http://dx.doi.org/10.1144/sjg15020139.

Blum, J.D., Erel, Y., 1995. A silicate weathering mechanism linking increases in marine $^{87}Sr/^{86}Sr$ with global glaciation. Nature. http://dx.doi.org/10.1038/373415a0.

Blum, J.D., Erel, Y., Brown, K., 1993. $^{87}Sr/^{86}Sr$ ratios of Sierra Nevada stream waters: implications for relative mineral weathering rates. Geochim. Cosmochim. Acta 58, 5019–5025.

Bradley, S.L., Milne, G.A., Shennan, I., Edwards, R., 2011. An improved glacial isostatic adjustment model for the British Isles. J. Quat. Sci. 26, 541–552. http://dx.doi.org/10.1002/jqs.1481.

Broecker, W.S., Bond, G., Klas, M., Clark, E., McManus, J., 1992. Origin of northern Atlantic's Heinrich events. Clim. Dyn. 6, 265–273.

Buggle, B., Glaser, B., Hambach, U., Gerasimenko, N., Markovi, S., 2011. An evaluation of geochemical weathering indices in loess–paleosol studies. Quat. Int. 240. http://dx.doi.org/10.1016/j.quaint.2010.07.019.

Carr, J.R., Vieli, A., Stokes, C.R., Jamieson, S.S.R., Palmer, S.J., Christoffersen, P., Dowdeswell, J.A., Nick, F.M., Blankenship, D.D., Young, D.A., 2015. Basal topographic controls on rapid retreat of Humboldt Glacier, northern Greenland. J. Glaciol. 61, 137–150. http://dx.doi.org/10.3189/2015JoG14J128.

Chen, J., An, Z., Head, J., 1999. Variation of Rb/Sr ratios in the loess-paleosol sequences of central China during the last 130,000 years and their implications for monsoon paleoclimatology. Quat. Res. 51, 215–219. https://doi.org/10.1006/qres.1999.2038.

Christensen, J.N., Halliday, A.N., Godfrey, L.V., Hein, J.R., Rea, D.K., 1997. Climate and ocean dynamics and the lead isotopic records in Pacific ferromanganese crusts. Science 277, 913–918.

Clark, P.U., 1987. Subglacial sediment dispersal and till composition. J. Geol. 95, 527–541.

Clark, C.D., Hughes, A.L.C., Greenwood, S.L., Jordan, C.J., Sejrup, H.P., 2012a. Pattern and timing of retreat of the last British-Irish Ice Sheet. Quat. Sci. Rev. 44, 112–146. http://dx.doi.org/10.1016/j.quascirev.2010.07.019.

Clark, J., McCabe, A.M., Bowen, D.Q., Clark, P.U., 2012b. Response of the Irish Ice Sheet to abrupt climate change during the last deglaciation. Quat. Sci. Rev. 35, 100–115. http://dx.doi.org/10.1016/j.quascirev.2012.01.001.

Clayburn, J.A.P., 1988. The crustal evolution of Central Scotland and the nature of the lower crust: Pb, Nd and Sr isotope evidence from Caledonian granites. Earth Planet. Sci. Lett. 90, 41–51.

Clayburn, J.A.P., Harmon, R.S., Pankhurst, R.J., Brown, J.F., 1983. Sr, O, and Pb isotope evidence for origin and evolution of Etive Igneous Complex, Scotland. Nature 303, 492–497.

Colville, E.J., Carlson, A.E., Beard, B.L., Hatfield, R.G., Stoner, J.S., Reyes, A.V., Ullman, D.J., 2011. Sr-Nd-Pb isotope evidence for ice-sheet presence on southern Greenland during the Last Interglacial. Science 333, 620–623.

Cook, A.J., 2005. Retreating glacier fronts on the Antarctic Peninsula over the past half-century. Science 308, 541–544. http://dx.doi.org/10.1126/science.1104235.

Crocket, K.C., Vance, D., Foster, G.L., Richards, D.a., Tranter, M., 2012. Continental weathering fluxes during the last glacial/interglacial cycle: insights from the marine sedimentary Pb isotope record at Orphan Knoll, NW Atlantic. Quat. Sci. Rev. 38, 89–99. http://dx.doi.org/10.1016/j.quascirev.2012.02.004.

Crocket, K.C., Foster, G.L., Vance, D., Richards, D.a., Tranter, M., 2013. A Pb isotope tracer of ocean-ice sheet interaction: the record from the NE Atlantic during the Last Glacial/Interglacial cycle. Quat. Sci. Rev. 82, 133–144. http://dx.doi.org/10.1016/j.quascirev.2013.10.020.

Dickin, A.P., 1981. Isotope geochemistry of tertiary igneous rocks from the Isle of Skye, N.W. Scotland. J. Petrol. 22, 155–189. http://dx.doi.org/10.1093/petrology/22.2.155.

Dickin, A.P., Exley, R.A., 1981. Isotopic and geochemical evidence for magma mixing in the petrogenesis of the Coire Uaigneich Granophyre, Isle of Skye, N.W. Scotland. Contrib. Mineral. Petrol. 76, 98–108. http://dx.doi.org/10.1007/BF00373689.

Dickin, A.P., Jones, N.W., 1983. Isotopic evidence for the age and origin of pitchstones and felsites, Isle of Eigg, NW Scotland. J. Geol. Soc. Lond. 140, 691–700.

Dickin, A.P., Moorbath, S., Welke, H.J., 1981. Isotope, trace element and major element geochemistry of Tertiary igneous rocks, Isle of Arran, Scotland. Earth Environ. Sci. Trans. R. Soc. Edinb. 72, 159–170. http://dx.doi.org/10.1017/S0263593300009974.

Dickin, A.P., Brown, J.L., Thompson, R.N., Halliday, A.N., Morrison, M.A., 1984. Crustal contamination and the granite problem in the British Tertiary Volcanic Province. Philos. Trans. R. Soc. Lond. 310, 755–780.

Dove, D., Arosio, R., Finlayson, A.G., Bradwell, T., Howe, J.A., 2015. Submarine glacial landforms record Late Pleistocene ice-sheet dynamics, Inner Hebrides, Scotland. Quat. Sci. Rev. 123, 76–90. http://dx.doi.org/10.1016/j.quascirev.2015.06.012.

Dowdeswell, J.A., Whittington, R.J., Jennings, A.E., Andrews, J.T., Mackensen, A., Marienfeld, P., 2000. An origin for laminated glacimarine sediments through sea-ice build-up and suppressed iceberg rafting. Sedimentology 47, 557–576.

Du, J., Haley, B.A., Mix, A.C., 2016. Neodymium isotopes in authigenic phases, bottom waters and detrital sediments in the Gulf of Alaska and their implications for paleo-circulation reconstruction. Geochim. Cosmochim. Acta 193, 14–35. http://dx.doi.org/10.1016/j.gca.2016.08.005.

Dunlop, P., Shannon, R., McCabe, A.M., Quinn, R., Doyle, E., 2010. Marine geophysical evidence for ice sheet extension and recession on the Malin Shelf: new evidence for the western limits of the British Irish Ice Sheet. Mar. Geol. 276, 86–99. http://dx.doi.org/10.1016/j.margeo.2010.07.010.

Emeleus, C.H., Bell, B.R., 2005. The palaeogene volcanic districts of Scotland. Brit. Geol. Surv.

Erel, Y., Morgan, J.J., 1992. The relationships between rock-derived lead and iron in natural waters. Geochim. Cosmochim. Acta 56, 4157–4167.

Evans, D.J.A., Phillips, E.R., Hiemstra, J.F., Auton, C.A., 2006. Subglacial till: formation, sedimentary characteristics and classification. Earth Sci. Rev. 78, 115–176. http://dx.doi.org/10.1016/j.earscirev.2006.04.001.

Fagel, N., Innocent, C., Gariepy, C., Hillaire-Marcel, C., 2002. Sources of Labrador Sea sediments since the last glacial maximum inferred from Nd-Pb isotopes. Geochim. Cosmochim. Acta 66, 2569–2581.

Farmer, G.L., Barber, D., Andrews, J.T., 2003. Provenance of Late Quaternary ice-prox-imal sediments in the North Atlantic: Nd, Sr and Pb isotopic evidence. Earth Planet. Sci. Lett. 209, 227–243. http://dx.doi.org/10.1016/S0012-821X(03)00068-2.

Finlayson, A.G., Fabel, D., Bradwell, T., Sugden, D.E., 2014. Growth and decay of a marine terminating sector of the last British-Irish Ice Sheet: a geomorphological re-construction. Quat. Sci. Rev. 83, 28–45. http://dx.doi.org/10.1016/j.quascirev.2013.10.009.

Floyd, P.A., Winchester, J.A., Park, R.G., 1989. Geochemistry and tectonic setting of Lewisian clastic metasediments from the Early Proterozoic Loch Maree Group of Gairloch, NW Scotland. Precambrian Res. 45, 203–214.

Font, L., Davidson, J.P., Pearson, D.G., Nowell, G.M., Jerram, D.A., Ottley, C.J., 2008. Sr and Pb isotope micro-analysis of plagioclase crystals from skye lavas: an insight into open-system processes in a flood basalt province. J. Petrol. 49, 1449–1471. http://dx.doi.org/10.1093/petrology/egn032.

Foster, G.L., Vance, D., 2006. Negligible glacial–interglacial variation in continental chemical weathering rates. Nature 444, 918–921. http://dx.doi.org/10.1038/nature05365.

Frost, C.D., O'Nions, R.K., 1985. Caledonian magma genesis and crustal recycling. J. Petrol. 26, 515–544. http://dx.doi.org/10.1093/petrology/26.2.515.

Geldmacher, J., Haase, K.M., Devey, C.W., Garbe-Schönberg, C.D., 1998. The petrogen-esis of Tertiary cone-sheets in Ardnamurchan, NW Scotland: petrological and geo-chemical constraints on crustal contamination and partial melting. Contrib. Mineral. Petrol. 131, 196–209.

Geldmacher, J., Troll, V.R., Emeleus, C.H., Donaldson, C.H., 2002. Pb-isotope evidence for contrasting crustal contamination of primitive to evolved magmas from Ardnamurchan and Rum: implications for the structure of the underlying crust. Scott. J. Geol. 38, 55–61. http://dx.doi.org/10.1144/sjg38010055.

Gibson, S.A., 1990. The geochemistry of the Trotternish sills, Isle of Skye: crustal con-tamination in the British Tertiary Volcanic Province. J. Geol. Soc. Lond. 147, 1071–1081.

Gutjahr, M., Frank, M., Stirling, C.H., Klemm, V., van de Flierdt, T., Halliday, A.N., 2007. Reliable extraction of a deepwater trace metal isotope signal from Fe-Mn oxyhydr-oxide coatings of marine sediments. Chem. Geol. 242, 351–370. http://dx.doi.org/10.1016/j.chemgeo.2007.03.021.

Gutjahr, M., Frank, M., Halliday, A.N., Keigwin, L.D., 2009. Retreat of the Laurentide ice sheet tracked by the isotopic composition of Pb in western North Atlantic seawater during termination 1. Earth Planet. Sci. Lett. 286, 546–555. http://dx.doi.org/10.1016/j.epsl.2009.07.020.

Gwiazda, R.H., Hemming, S.R., Broecker, W.S., 1996a. Tracking the sources of icebergs with lead isotopes: the provenance of ice-rafted debris in Heinrich layer 2. Paleoceanography 11, 77–93. http://dx.doi.org/10.1029/95PA03135.

Gwiazda, R.H., Hemming, S.R., Broecker, W.S., 1996b. Provenance of icebergs during Heinrich event 3 and the contrast to their sources during other Heinrich episodes. Paleoceanography 11, 371–378.

Hamilton, P.J., Evensen, N.M., O'Nions, R.K., 1979. Sm-Nd systematics of Lewisian gneisses: implications for the origin of granulites. Nature 277, 25–28.

Harlavan, Y., Erel, Y., 2002. The release of Pb and REE from granitoids by the dissolution of accessory phases. Geochim. Cosmochim. Acta 66, 837–848. http://dx.doi.org/10.1016/S0016-7037(01)00806-7.

Hein, J.R., Gibbs, A.E., Clague, D.A., Torresan, M., 1996. Hydrothermal mineralization along submarine rift zones, Hawaii. Mar. Georesour. Geotechnol. 14, 177–203. http://dx.doi.org/10.1080/10641199609388310.

Hemming, S.R., 2004. Heinrich events: massive late Pleistocene detritus layers of the North Atlantic and their global climate imprint. Rev. Geophys. 42. http://dx.doi.org/10.1029/2003RG000128.1.INTRODUCTION.

Howe, J.A., Dove, D., Bradwell, T., Gafeira, J., 2012. Submarine geomorphology and glacial history of the Sea of the Hebrides, UK. Mar. Geol. 315–318, 64–76. http://dx.doi.org/10.1016/j.margeo.2012.06.005.

Inall, M., Gillibrand, P., Griffiths, C., MacDougal, N., Blackwell, K., 2009. On the ocea-nographic variability of the North-West European Shelf to the West of Scotland. J. Mar. Syst. 77, 210–226. http://dx.doi.org/10.1016/j.jmarsys.2007.12.012.

Jamieson, S.S.R., Vieli, A., Ó Cofaigh, C., Stokes, C.R., Livingstone, S.J., Hillenbrand, C.D., 2014. Understanding controls on rapid ice-stream retreat during the last de-glaciation of Marguerite Bay, Antarctica, using a numerical model. J. Geophys. Res. Earth Surf. 119, 247–263. http://dx.doi.org/10.1002/2013JF002934.

Johnson, K., Johnson, B., Johnson, H., 2016. Periodic Table of Elements in the Ocean (PTEO) [WWW Document]. URL. http://www.mbari.org/science/upper-ocean-systems/chemical-sensor-group/periodic-table-of-elements-in-the-ocean/.

Johnstone, G.S., Plant, J., Watson, J.V., 1979. Caledonian granites in relation to regional geochemistry in northern Scotland. Geol. Soc. Lond., Spec. Publ. 8, 663–667.

Joughin, I., Tulaczyk, S., Bindschadler, R., Price, S.F., 2002. Changes in west Antarctic ice stream velocities: observation and analysis. J. Geophys. Res. 107, 1–22. http://dx.doi.org/10.1029/2001JB001029.

Joughin, I., Smith, B.E., Medley, B., 2014. Marine ice sheet collapse potentially underway for the Thwaites Glacier Basin, West Antarctica. Science (New York, N.Y.) 344, 735–738. http://dx.doi.org/10.1126/science.1249055.

Kerr, A.C., Kempton, P.D., Thompson, R.N., 1995. Crustal assimilation during turbulent magma scent (ATA); new isotopic evidence from the Mull Tertiary lava succession, N.W. Scotland. Contrib. Mineral. Petrol. 119, 142–154.

Klovan, J.E., Billings, G.K., 1967. Classification of geological samples by discriminant-function analysis. Bull. Can. Petrol. Geol. 15, 313–330.

Knutz, P.C., Austin, W.E.N., John, W., Jones, E., 2001. Millennial-scale depositional cy-cles related to British ice sheet variability and North Atlantic paleocirculation since 45 kyr B.P., Barra Fan, U.K. margin. Paleoceanography 16, 53–64. http://dx.doi.org/10.1029/1999PA000483.

Kurzweil, F., Gutjahr, M., Vance, D., Keigwin, L., 2010. Authigenic Pb isotopes from the Laurentian Fan: changes in chemical weathering and patterns of North American freshwater runoff during the last deglaciation. Earth Planet. Sci. Lett. 299, 458–465. http://dx.doi.org/10.1016/j.epsl.2010.09.031.

Lambert, R.S.J., Winchester, J.A., Holland, J.G., 1981. Comparative geochemistry of pelites from the Moinian and Appin Group (Dalradian) of Scotland. Geol. Mag. 118, 477–490.

Lambert, R.S.J., Holland, J.G., Winchester, J.A., 1982. A geochemical comparison of the Dalradian Leven Schists and the Grampian Division Monadhliath Schists of Scotland. J. Geol. Soc. 139, 71–84.

Larsen, B., 1983. Geology of the Greenland-Iceland Ridge in the Denmark Strait. In: Bott, M.H.P., Saxov, S., Talwani, M., Thiede, J. (Eds.), Structure and Development of the Greenland-Scotland Ridge. Plenum Publishing Corporation, London, pp. 425–444.

Maccali, J., Hillaire-Marcel, C., Carignan, J., Reisberg, L.C., 2012. Pb isotopes and geo-chemical monitoring of Arctic sedimentary supplies and water mass export through Fram Strait since the Last Glacial Maximum. Paleoceanography 27. http://dx.doi.org/10.1029/2011PA002152.

McCabe, A.M., Williams, G.D., 2012. Timing of the East Antrim Coastal Readvance: phase relationships between lowland Irish and upland Scottish ice sheets during the Last Glacial Termination. Quat. Sci. Rev. 58, 18–29. http://dx.doi.org/10.1016/j.quascirev.2012.10.012.

Moorbath, S., Welke, H.J., Gale, N.H., 1969. The significance of lead isotope studies in ancient, high-grade metamorphic basement complexes, as exemplified by the Lewisian rocks of Northwest Scotland. Earth Planet. Sci. Lett. 6, 245–256.

Moorbath, S., Powell, J.L., Taylor, P.N., 1975. Isotopic evidence for the age and origin of the "grey gneiss" complex of the southern Outer Hebrides, Scotland. J. Geol. Soc. Lond. 131, 213–222.

Muir, R.J., Evans, J.A., Fitches, W.R., 1993. Mafic dykes within the Lewisian Complex on Tiree and Coll, Inner Hebrides. Scott. J. Geol. 29, 167–176.

Patton, H., Hubbard, A., Andreassen, K., Winsborrow, M., Stroeven, A.P., 2016. The build-up, configuration, and dynamical sensitivity of the Eurasian ice-sheet complex to Late Weichselian climatic and oceanic forcing. Quat. Sci. Rev. 153, 97–121. http://dx.doi.org/10.1016/j.quascirev.2016.10.009.

Poulton, S.W., Canfield, D.E., 2005. Development of a sequential extraction procedure for iron: implications for iron partitioning in continentally derived particulates. Chem. Geol. 214, 209–221. http://dx.doi.org/10.1016/j.chemgeo.2004.09.003.

Preston, R.J., Bell, B.R., Rogers, G., 1998. The Loch Scridain Xenolithic Sill Complex, Isle of Mull, Scotland: fractional crystallization, assimilation, magma-mixing and crustal anatexis in subvolcanic conduits. J. Petrol. 39, 519–550.

Pritchard, H.D., Arthern, R.J., Vaughan, D.G., Edwards, L.A., 2009. Extensive dynamic thinning on the margins of the Greenland and Antarctic ice sheets. Nature 461, 971–975. http://dx.doi.org/10.1038/nature08471.

Raiswell, R., 2011. Iceberg-hosted nanoparticulate Fe in the Southern Ocean: Mineralogy, origin, dissolution kinetics and source of bioavailable Fe. Deep-Sea Res. II Top. Stud. Oceanogr. 58, 1364–1375. http://dx.doi.org/10.1016/j.dsr2.2010.11.011.

Raiswell, R., Tranter, M., Benning, L.G., Siegert, M., De'ath, R., Huybrechts, P., Payne, T., 2006. Contributions from glacially derived sediment to the global iron (oxyhydr) oxide cycle: implications for iron delivery to the oceans. Geochim. Cosmochim. Acta 70, 2765–2780. http://dx.doi.org/10.1016/j.gca.2005.12.027.

Raiswell, R., Benning, L.G., Davidson, L., Tranter, M., Tulaczyk, S., 2009. Schwertmannite in wet, acid, and oxic microenvironments beneath polar and polythermal glaciers. Geology 37 (5), 431–434. http://dx.doi.org/10.1130/G25350A.1.

Reimer, P.J., Bard, E., Bayliss, A., Beck, J.W., Blackwell, P.G., Ramsey, C.B., 2013. IntCal13 and Marine13 radiocarbon age calibration curves 0–50,000 years cal BP. Radiocarbon 55, 1869–1887. http://dx.doi.org/10.2458/azu_js_rc.55.16947.

Scourse, J.D., Haapaniemi, A.I., Colmenero-Hidalgo, E., Peck, V.L., Hall, I.R., Austin, W.E.N., Knutz, P.C., Zahn, R., 2009. Growth, dynamics and deglaciation of the last British-Irish ice sheet: the deep-sea ice-rafted detritus record. Quat. Sci. Rev. 28, 3066–3084. http://dx.doi.org/10.1016/j.quascirev.2009.08.009.

Shipp, S.S., Wellner, J.S., Anderson, J.B., 2002. Retreat signature of a polar ice stream: sub-glacial geomorphic features and sediments from the Ross Sea, Antarctica. Geol. Soc. Lond., Spec. Publ. 203, 277–304. http://dx.doi.org/10.1144/GSL.SP.2002.203.01.15.

Small, D., Parrish, R.R., Austin, W.E.N., Cawood, P.A., Rinterknecht, V., 2013. Provenance of North Atlantic ice-rafted debris during the last deglaciation-a new application of U-Pb rutile and zircon geochronology. Geology 41, 155–158. http://dx.doi.org/10.1130/G33594.1.

Small, D., Benetti, S., Dove, D., Ballantyne, C.K., Fabel, D., Clark, C.D., Gheorghiu, D., Newall, J., Xu, S., 2017. Cosmogenic exposure age constraints on deglaciation and flow behaviour of a marine-based ice stream in western Scotland, 21–16 ka. Quat. Sci. Rev. 167, 30–46.

Stone, J.O., Ballantyne, C.K., 2006. Dimensions and deglacial chronology of the Outer Hebrides Ice Cap, northwest Scotland: implications of cosmic ray exposure dating. J. Quat. Sci. 21, 75–84. http://dx.doi.org/10.1002/jqs.933.

Stuiver, M., Reimer, P.J., Reimer, R.W., 2016. CALIB 7.1.

Tanaka, T., Togashi, S., Kamioka, H., Amakawa, H., Kagami, H., Hamamoto, T., Yuhara, M., Orihashi, Y., Yoneda, S., Shimizu, H., Kunimaru, T., Takahashi, K., Yanagi, T., Nakano, T., Fujimaki, H., Shinjo, R., Asahara, Y., Tanimizu, M., Dragusanu, C., 2000. JNdi-1: a neodymium isotopic reference in consistency with LaJolla neodymium. Chem. Geol. 168, 279–281. http://dx.doi.org/10.1016/S0009-2541(00)00198-4.

Taylor, S.R., McLennan, S.M., 1995. The geochemical evolution of the continental crust. Rev. Geophys. 33, 241–265. http://dx.doi.org/10.1029/95RG00262.

Tessier, A., Campbell, P.G.C., Bisson, M., 1979. Sequential extraction procedure for the speciation of particulate trace metals. Anal. Chem. 51, 844–851. http://dx.doi.org/10.1021/ac50043a017.

Thirlwall, M.F., 1982. Systematic variation in chemistry and Nd-Sr isotopes across a Caledonian calc-alkaline volcanic arc: implications for source materials. Earth Planet. Sci. Lett. 58, 27–50.

Thirlwall, M.F., 1986. Lead isotope evidence for the nature of the mantle beneath Caledonian Scotland. Earth Planet. Sci. Lett. 80, 55–70. http://dx.doi.org/10.1016/0012-821X(86)90019-1.

Thirlwall, M.F., 1991. Long-term reproducibility of multicollector Sr and Nd isotope ratio analysis. Chem. Geol. 94, 85–104. http://dx.doi.org/10.1016/0168-9622(91)90002-E.

Thornalley, D.J.R., Barker, S., Broecker, W.S., Elderfield, H., McCave, I.N., 2011. The deglacial evolution of North Atlantic deep convection. Science 331, 202–205. http://dx.doi.org/10.1126/science.1196812.

Trewin, N.H., 2002. The geology of Scotland. In: Geological Society of London, 4th ed. .

Uehara, K., Scourse, J.D., Horsburgh, K.J., Lambeck, K., Purcell, A.P., 2006. Tidal evolution of the northwest European shelf seas from the Last Glacial Maximum to the present. J. Geophys. Res. 111, C09025. http://dx.doi.org/10.1029/2006JC003531.

Van De Kamp, P.C., 1970. The Green Beds of the Scottish Dalradian Series: geochemistry, origin, and metamorphism of mafic sediments. J. Geol. 78, 281–303.

von Blanckenburg, F., Nägler, T.F., 2001. Weathering versus circulation-controlled changes in radiogenic isotope tracer composition of the Labrador Sea and North Atlantic Deep Water. Paleoceanography 16, 424–434.

Ward, S.L., Neill, S.P., Scourse, J.D., Bradley, S.L., Uehara, K., 2016. Sensitivity of palaeotidal models of the northwest European shelf seas to glacial isostatic adjustment since the Last Glacial Maximum. Quat. Sci. Rev. 151, 198–211. http://dx.doi.org/10.1016/j.quascirev.2016.08.034.

Weaver, B.L., Tarney, J., 1980. Rare Earth geochemistry of Lewisian granulite-facies gneisses, northwest Scotland: implications for the petrogenesis of the Archaean lower continental crust. Earth Planet. Sci. Lett. 51, 279–296.

Wilson, L.J., Austin, W.E.N., Jansen, E., 2002. The last British Ice Sheet: growth, maximum extent and deglaciation. Polar Res. 21, 243–250.